

**EFFECTS OF MECHANICAL FORCES ON CYTOSKELETAL REMODELING
AND STIFFNESS OF CULTURED SMOOTH MUSCLE CELLS**

A Dissertation

by

SUNGSOO NA

Submitted to the Office of Graduate Studies of
Texas A&M University
in partial fulfillment of the requirements for the degree of

DOCTOR OF PHILOSOPHY

May 2006

Major Subject: Biomedical Engineering

**EFFECTS OF MECHANICAL FORCES ON CYTOSKELETAL REMODELING
AND STIFFNESS OF CULTURED SMOOTH MUSCLE CELLS**

A Dissertation

by

SUNGSOO NA

Submitted to the Office of Graduate Studies of
Texas A&M University
in partial fulfillment of the requirements for the degree of

DOCTOR OF PHILOSOPHY

Approved by:

Chair of Committee,	Jay D. Humphrey
Committee Members,	John C. Criscione
	Wonmuk Hwang
	Gerald A. Meininger
	Hsin-i Wu
Head of Department,	Gerald L. Cote'

May 2006

Major Subject: Biomedical Engineering

ABSTRACT

Effects of Mechanical Forces on Cytoskeletal Remodeling
and Stiffness of Cultured Smooth Muscle Cells. (May 2006)

Sungsoo Na, B.S., Pukyong National University;

M.S., Pusan National University

Chair of Advisory Committee: Dr. Jay D. Humphrey

The cytoskeleton is a diverse, multi-protein framework that plays a fundamental role in many cellular activities including mitosis, cell division, intracellular transport, cell motility, muscle contraction, and the regulation of cell polarity and organization. Furthermore, cytoskeletal filaments have been implicated in the pathogenesis of a wide variety of diseases including cancer, blood disease, cardiovascular disease, inflammatory disease, neurodegenerative disease, and problems with skin, nail, cornea, hair, liver and colon. Increasing evidence suggests that the distribution and organization of the cytoskeleton in living cells are affected by mechanical stresses and the cytoskeleton determines cell stiffness.

We developed a fully nonlinear, constrained mixture model for adherent cells that allows one to account separately for the contributions of the primary structural constituents of the cytoskeleton and extended a prior solution from the finite elasticity literature for use in a sub-class of atomic force microscopy (AFM) studies of cell mechanics. The model showed that the degree of substrate stretch and the geometry of the AFM tip dramatically affect the measured cell stiffness. Consistent with previous

studies, the model showed that disruption of the actin filaments can reduce the stiffness substantially, whereas there can be little contribution to the overall cell stiffness by the microtubules or intermediate filaments. To investigate the effect of mechanical stretching on cytoskeletal remodeling and cell stiffness, we developed a simple cell-stretching device that can be combined with an AFM and confocal microscopy. Results demonstrate that cyclic stretching significantly and rapidly alters both cell stiffness and focal adhesion associated vinculin and paxillin, suggesting that focal adhesion remodeling plays a critical role in cell stiffness by recruiting and anchoring F-actin. Finally, we estimated cytoskeletal remodeling by synthesizing data on stretch-induced dynamic changes in cell stiffness and focal adhesion area using constrained mixture approach. Results suggest that the acute increase in stiffness in response to an increased cyclic stretch was probably due to an increased stretch of the original filaments whereas the subsequent decrease back towards normalcy was consistent with a replacement of the highly stretched original filaments with less stretched new filaments.

ACKNOWLEDGMENTS

I would like to express my gratitude to all those without whom this dissertation would not have been possible. I am deeply indebted to my advisor, Dr. Jay Humphrey who is my mentor and a role model as a researcher, a teacher, a father and a husband. His patience and encouragement have carried me on through difficult times and his constant support, invaluable suggestions, and insightful discussions make all my research possible. I am greatly grateful to my committee members, Dr. Gerald Meininger, for allowing me to use his lab equipments whenever I need, Dr. John Criscione for his advice about continuum mechanics, which was crucial for my first project, Dr. Wonmuk Hwang for stimulating discussions about cytoskeletal remodeling, and Dr. Hsin-I Wu, for his valuable suggestions to my research.

I have been so blessed to have great labmates. I would like to acknowledge Drs. Zhe Sun and Andreea Trache in Dr. Meininger's lab who spent significant time helping me learn all lab work from the beginning, Dr. Seungik Baek for meaningful talks about theoretical modeling, Dr. Paul Wells and Ryan Pedrigi for helping me calibrate the cell extension device. Financial support from the Fred J. Benson Graduate Fellowship, the Whitaker Foundation, and the National Institute of Health is gratefully acknowledged.

I am deeply grateful to my parents and family who trust me and provide endless support for me. Especially, I would like to give special thanks to my wife, Heejung Hwang for her love, patience, and considerate support to complete this work.

Above all supports, I greatly thank my God for giving me all opportunities and precious people and allowing me to know Him more through his creation.

TABLE OF CONTENTS

	Page
ABSTRACT	iii
ACKNOWLEDGMENTS.....	v
TABLE OF CONTENTS	vii
LIST OF FIGURES.....	ix
LIST OF TABLES	xi
CHAPTER	
I INTRODUCTION.....	1
II ATOMIC FORCE MICROSCOPY AND THE CONSTITU- TIVE BEHAVIOR OF LIVING CELLS	9
Introduction	9
Background	12
New theoretical framework.....	18
Illustrative simulations	24
Discussion	31
III TIME-DEPENDENT CHANGES IN CELL STIFFNESS AND FOCAL ADHESION AREA IN RESPONSE TO CYCLIC STRETCH	35
Introduction	35
Materials and methods	37
Results	46
Discussion	55

CHAPTER	Page
IV	
TIME-DEPENDENT CHANGES IN CYTOSKELETAL REMODELING IN RESPONSE TO CYCLIC STRETCH: A THEORETICAL STUDY BASED ON EXPERIMENTAL DATA.....	61
Introduction.....	61
Materials and methods.....	62
Results.....	69
Discussion.....	76
V	
SUMMARY AND CONCLUSIONS.....	83
REFERENCES.....	89
APPENDIX.....	98
VITA.....	100

LIST OF FIGURES

FIGURE		Page
2.1	Deflection image of a vascular smooth muscle cell isolated from the rat skeletal muscle arterioles.....	10
2.2	Local spherical coordinate system used for microstructurally-motivated, phenomenological constitutive relations of a living cell.....	20
2.3	Four configurations for an adherent cell, including an assumed materially isotropic cell in a non-adherent, traction-free reference configuration.....	21
2.4	Illustrative (possible) distributions of cytoskeletal filaments given by a von Mises-Fisher distribution function.....	26
2.5	Combined out-of-plane indentation and in-plane equibiaxial stretch for (A) exponential-type filaments and (B) linear-type filaments, each indented by a flat-ended circular cylinder with radius 30 nm.....	29
2.5	Combined indentation and equibiaxial in-plane stretch, $\mu = 1.2$, for the exponential-type filament behavior.....	30
3.1	Schema of the cell extension device.....	38
3.2	(A) Placement of tracking markers for calibration of membrane stretch as a function of pump volume. Seven sets of four markers are placed on the membrane to confirm homogeneous and equibiaxial stretch. (B) Calibration plot of the mean equibiaxial stretch versus the volume of air infused/withdrawn.....	40
3.3	(A) Stretch ratios at various positions along the radius of the membrane. The stretch field is nearly homogeneous, particularly in the central 40% of the membrane, the mean value of which is shown by horizontal dashed line. (B) Stretch ratios in two orthogonal directions (X and Y) in the center during air withdrawal from 1 to 5 ml.....	42

FIGURE	Page
3.4 Time course of changes in cell stiffness during AFM indentation measurement.....	47
3.5 Effect of tip geometry on cell stiffness	48
3.6 Each bar shows stiffness (mean \pm SD) of individual cells subjected to 10% cyclic stretching.....	50
3.7 Effect of cyclic stretching time and magnitude on cell stiffness	52
3.8 Immunofluorescence micrographs of rat vascular smooth muscle cells	53
3.9 Effect of equibiaxial stretch on focal contact localization	54
3.10 Ratio of FA associated vinculin (open) and paxillin (shaded) area to corresponding projected cell area in response to stretching time	56
3.11 Correlation between cell stiffness and FA associated vinculin/paxillin area ratio in response to 10% cyclic stretch.....	57
4.1 Flow chart showing a synthesis of experiments and modeling	63
4.2 Effects of equibiaxial stretch on FA localization	70
4.3 Data from thirteen force-indentation tests obtained from AFM indentations of unstretched cells were fitted with a CSK remodeling model (solid line) to estimate mass fraction of F-actin in unstretched state.....	72
4.4 CSK remodeling in response to cyclic stretching	75
4.5 Representative force-indentation curves fitted with AFM indentation measurements obtained from independent experiments: (A) unstretch; (B) 2 min of 10% cyclic stretch; (C) 30 min of 10% cyclic stretch	79

LIST OF TABLES

TABLE		Page
2.1	Material parameters for a model cell.....	28
4.1	FA associated vinculin area ratios and total mass fractions of F-actin in response to 10% cyclic stretching.....	73

CHAPTER I

INTRODUCTION

Mechanical stimuli on cells, including fluid-induced shear or matrix-induced stretch, can affect signal transduction and altered gene expression, which in turn alter migration, proliferation, adhesion, and host of other cellular responses (Goldschmidt et al., 2001; Li and Xu, 2000; Reusch et al., 1996; Kim et al., 1999; Sumpio et al., 1987). These functional alterations are mediated through changes in the intracellular structure known as the cytoskeleton (CSK), which is responsible for the structured integrity and mechanical links between the nucleus and surface adhesion receptors. Increasing evidence suggests that the distribution and organization of the CSK in living cells are affected by mechanical stresses (Smith et al., 1997; Galbraith et al., 1998; Takemasa et al., 1998; Wang et al., 2000, 2001; Hayakawa et al., 2001; Costa et al., 2002; Yoshigi et al., 2003). For example, using western blots showed that stretching the vascular wall induces actin filament (F-actin) polymerization in smooth muscle cells (Albinsson et al., 2004). Using similar methods, Cunningham et al. (2002) quantified focal contact associated proteins in smooth muscle cells subjected to cyclic strain, and suggested that insoluble levels of focal contact components are altered rapidly following an appropriate number of mechanical perturbations.

It is generally accepted that the CSK is the major determinant of cell stiffness, particularly the F-actin (Wu et al., 1998a; Smith et al., 2003; Huang et al., 2005). In

This dissertation follows the style of Journal of Biomechanics.

particular, disrupting the F-actin network with cytochalasin D reduces cell stiffness by ~50%. In contrast, glutaraldehyde (a common histological fixative) increases cell stiffness up to three fold by increasing the degree of crosslinking between F-actin and the rest of the CSK network (Wu et al., 1998a). In focal adhesions (FAs), F-actin is linked to transmembrane proteins called integrins via a variety of proteins, including paxillin and vinculin. Goldmann et al. (1998) showed, for example, that the stiffness of vinculin-deficient cells was lower than that of wild-type cells; when vinculin expression was reinstated by transfer of the gene encoding vinculin, cell stiffness was attained close to that of the wild-type cells. These results point to a role for vinculin in stabilizing FA and transferring mechanical stress from the extracellular matrix (ECM) to the CSK network.

Changes in cellular function due to disease are also often mirrored in the CSK. For example, CSK alterations cause capillary clogs in circulatory disorders (Worthen et al., 1989); changes in CSK from a rather ordered and stiff structure to a more irregular and compliant one during a cell's progression from a fully mature state to a replicating, motile, and immortal cancerous cell include a reduction in CSK structure and its accessory proteins (Ben-zé'ev, 1985). Clearly, changes in CSK content and structure should be reflected in the overall mechanical properties of the cell. Therefore, the mechanical properties of certain types of cells may potentially be used to quantitatively reflect the state of their CSK structure and health, which could be useful in possible applications in clinical diagnostics of certain types of diseases.

Mechanical properties of cells have been studied extensively given the recent development of experimental techniques capable of probing and manipulating forces and displacements less than a piconewton and a nanometer, respectively. Micropipette aspiration has been a prevalent technique (Hochmuth, 2000). Here, the cell is drawn into the mouth of the pipette via the stepwise application of an aspiration pressure. This pressure is maintained for a specified duration, and the attendant extension of the cell into the pipette is monitored via optical microscopy. This permits stress-strain properties to be estimated, although the dominant effect is due to the membrane. The microneedle technique is another early experimental approach, whereby portions of the cell are deformed via a cantilevered probe and displacement is measured optically (Felder and Elson, 1990). Thus, this technique is dependent on the stiffness of cantilever and optically obtained displacement resolution. Embedded particle tracking has been used to measure traction forces exerted by adherent cells (Munevar et al., 2001; Butler et al., 2002). Here, fluorescent beads (0.2 μm in diameter) embedded in the gel serve as fiduciary markers within a flexible membrane. The displacement of the beads is measured optically, and the corresponding traction between the adherent cell and its substrate is computed from the given displacement field. Several experimental techniques using photon momentum (Ashkin and Dziedzic, 1987) have become popular. Optical traps, also called optical tweezers, laser tweezers or laser traps, consist of a laser directed at a micrometer-scale object, such as beads or organelles; the laser beam is used both to control the position of the bead and to measure the required force. Typically, two beads are positioned at opposite ends of the cell. The position of one cell-attached bead

is fixed to a stationary glass slide while the opposite cell-attached bead is confined by moving the optical trap, the position of which is modulated via the magnitude of the laser power. A variation of an optical trap is called an optical stretcher. In this technique, two lasers expose diametrically opposite portions of the cell, but are not focused in a plane. These unfocused lasers exert net forces due to refraction when a laser beam enters and exits the cell surface. Displacement of the cell is measured directly via image analysis, and the corresponding force is calculated via geometric ray optics as a function of light reflected and total light power.

Magnets have also been used to apply either a linear force or a twisting torque to a particle that is affixed to or embedded in a cell. In the case of a linear force application, magnetic beads serve as “grips” which, under electromagnetic field gradients that impose a local magnetic force on these beads, impose displacement (Goldschmidt et al., 2001). An important variation is to apply a magnetic torque (Wang et al, 1993). This technique is termed magnetic twisting cytometry. Here, large numbers of magnetic beads are coated with ligands chosen specifically to bind to cell surface receptors such as integrins that interact with the CSK. After these ligand-coated beads are introduced to the cell, a weak magnetic field is applied on the sample to magnetize the beads with a specific orientation. When a counterpulse is generated at a much higher magnitude and in a different direction, the beads then experience a rotational force and realign with new magnetic field. One application of magnetic twisting cytometry has been to estimate the storage modulus and loss modulus (within a linear viscoelastic framework) of human airway smooth muscle cells (Deng et al., 2004). Finally, atomic force microscopy

(AFM) was originally developed as a high-resolution imaging instrument (i.e., sensitive profilometer) by monitoring the deflection of a small cantilever probe as its tip raster-scanned over a sample surface. AFM has become an important tool for mechanobiology studies, however, because it can be used in multiple modes in physiologic aqueous solutions in conjunction with light and fluorescence microscopy. More recently, AFM has been used to estimate a cell stiffness (Rotsch and Radmacher, 2000; Mathur et al., 2001; Na et al., 2004), to estimate adhesion forces of ligand-receptor pairs (Sun et al., 2005), to image underlying CSK structures (Kuznetsov et al., 1997), and to study single cell calcium signaling in response to mechanical strain (Charras and Horton, 2002).

Taken together, the mechanical properties of cells and CSK remodeling in response to altered mechanical stress have been studied extensively given the recent development of techniques capable of probing and manipulating forces and displacements less than a piconewton and a nanometer, respectively. Nonetheless, little is known about the quantitative relationship between the mechanical properties of cells and CSK remodeling.

Prior mathematical models have been derived using either the continuum approach or the microstructural approach (for a review, see Humphrey, 2002; Stamenovic and Ingber, 2002). The former treats the cell as comprising constituents with certain continuum material properties (e.g., Evans and Yeung, 1989; Schmid-Schönbein et al., 1995). On the other hand, microstructural approaches assume the CSK is the main structural component. This approach is especially developed for investigating CSK mechanics in adherent cells (e.g. Boey et al., 1998; Forgacs, 1995; Satcher and Dewey,

1996; Stamenovic et al., 1996). The cortical membrane model depicts a structurally significant membrane surrounding a liquid cytoplasm (Evans and Yeung, 1989). It rests on the assumption that there is a cortex with a finite thickness and bending rigidity or an internal structure on the cytoplasmic side of the plasma membrane which maintains the curvature (Schmid-Schönbein et al., 1995), and that mechanical state of the cytoplasm, which is a single phase viscoelastic medium, determines the stress distribution in the cell. However, this assumption contradicts observations that mechanical stimuli on the cell surface are transmitted via molecular connectivity of the CSK. Ingber and colleagues suggested that eukaryotic cells display both CSK structure and elastic deformability that appear to be consistent with tensegrity where actin filaments and intermediate filaments play the role of tension-supporting cables and microtubules and actin bundles play the role of compression-supporting struts (Ingber, 1993). They have assumed that the cables representing actin filaments and intermediate filaments exhibit a linear elastic behavior. Forgacs (1995) employed a percolation theory to propose a possible mechanism for intracellular signaling. In a percolation model, the CSK is assumed to be interconnected network of actin filaments, microtubules, and intermediate filaments. A shortcoming of the percolation model is that it does not take CSK forces into consideration. Satcher and Dewey (1996) used an open-cell foam model to estimate the contribution of the actin lattice to the elastic behavior of cultured endothelial cells. They assumed that CSK forces arise from the deformation of individual CSK filaments (i.e. bending) that exhibit a linear elastic response under the action of mechanical stresses applied to the cell. Boey et al. (1998) examined three configurations of the

erythrocyte CSK using a polymer chain model: stress-free, prestressed, and condensed. Fabry et al. (2001) suggest that a sol-gel transition is required to describe dynamic properties of the cell: solid-like behavior is needed to maintain structural integrity of the cell, but fluid-like behavior is needed during cell movement. They suggest further that the effective noise temperature that comes from the physics of soft glassy materials is a measure of the CSK deformation and flow. Thus, rather than thinking of the CSK as a gel, this model suggests that it should be thought of as a glassy material close to a glass transition, and that disorder and metastability may be essential features underlying its mechanical functions. Recently, Humphrey (2002a) proposed a fundamentally different approach based on the concept of a constrained mixture, which is a microstructurally motivated continuum model that allows individual constituents to turnover dynamically. This approach allows one to include the separate contributions and distributions of the primary CSK filaments and viscous cytosol without having to solve separate balance relations for each constituent, to quantify possible momentum exchanges between constituents, or to prescribe partial traction boundary conditions which are notoriously difficult to identify. Thus, this approach can provide details on locally averaged distributions of stresses and strains in cells, which in turn can be useful in determining the distribution and transmission of these forces to subcellular components.

The overall objectives of this study were (a) to develop a constrained-mixture based constitutive model for cells that can predict CSK remodeling in response to mechanical stimulus, (b) to examine the time course of changes in cell stiffness and CSK remodeling in response to mechanical stimulus. To accomplish these goals, we developed a simple

cell-stretching device that can be combined with an atomic force microscope and a confocal microscope to examine the time course of changes in cell stiffness and CSK remodeling, respectively. Next, we used a constrained mixture approach to model CSK remodeling by synthesizing AFM data on stretch-induced dynamic changes in cell stiffness and confocal microscopy acquired data on changes in FA-related areas.

Results showed that cyclic stretching significantly and rapidly alters both cell stiffness and focal adhesion localization, suggesting that focal adhesion remodeling plays a critical role in cell stiffness by recruiting and anchoring F-actin, and the acute increase in stiffness in response to an increased cyclic stretch was probably due to an increased stretch of the original F-actin whereas the subsequent decrease back towards normalcy was consistent with a replacement of the highly stretched original F-actin with less stretched new F-actin.

CHAPTER II

ATOMIC FORCE MICROSCOPY AND THE CONSTITUTIVE BEHAVIOR OF LIVING CELLS*

Introduction

Among the myriad exciting discoveries of modern biology is the observation that many types of cells respond dramatically to changes in their mechanical environment. Such cells may alter their orientation, shape, internal constitution, contraction, migration, adhesion, synthesis and degradation of extracellular constituents, or even their life cycle in response to perturbations in mechanical loading (Zhu et al., 2000). Counted among these cell types are the chondrocytes, endothelial cells, epithelial cells, fibroblasts, macrophages, myocytes, and osteocytes, to name but a few. Although much has been learned about the mechanosensitive responses of living cells, there remains a pressing need for quantification and, in particular, for mathematically modeling the mechanobiology (Fung, 2002).

Atomic force microscopy is one of several new technologies that promise to increase our understanding of the mechanobiology and biomechanics of living cells (Radmacher et al., 1992). Briefly, the atomic force microscope (AFM) is a cantilever-based scanning probe that can be operated in two primary modes: the constant force mode allows the AFM to serve as a highly sensitive profilometer, thus enabling one to

* Reprinted with permission from “On atomic force microscopy and the constitutive behavior of living cells” by Na, S., Sun, Z., Meininger, G.A., Humphrey, J.D., 2004. *Biomechanics and Modeling in Mechanobiology*, 3, 75-84. Copyright 2004 by Springer-Verlag.

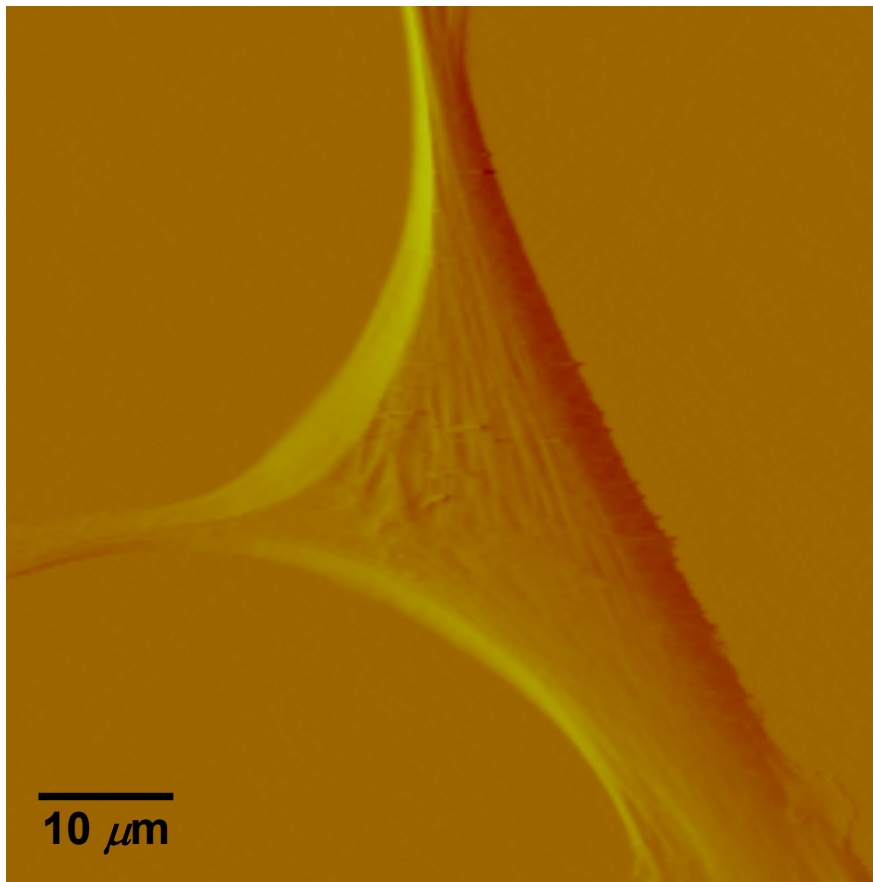


Fig. 2.1. Deflection image of a vascular smooth muscle cell isolated from the rat skeletal muscle arterioles. The AFM probe was scanned across the cell surfaces at a speed of 40 nm/s, with a tracking force of approximately 400 pN. The image was collected using Nanoscope III Software.

map the surface topography of a cell (Fig. 2.1.); the displacement mode allows one to perform mechanical tests on cells, particularly local indentation or local pulling following adhesion of the probe. The tip of the cantilever largely dictates the resolution and ‘sphere of influence’ of the mechanical interrogation. Tips can be micro-fabricated to have different sizes and shapes, but many are on the order of 10-50 nm and shaped either as a cone or a blunted-cone with a spherical cap. In the displacement mode,

common indentations are on the order of 50-500 nm, with the thickness of the cell often on the order of 1-3 μm .

Most AFM-based studies of the mechanical behavior of living cells (e.g., Wu et al., 1998a; Rotsch and Radmacher, 2000; Mathur et al., 2001) are interpreted using the classical Hertz solution for the indentation of an elastic half-space (e.g., Sneddon, 1965). This solution was derived, of course, within the context of the many simplifying assumptions of classical elasticity: linear elastic behavior, material uniformity and homogeneity, isotropy, and infinitesimal strains. Few of these assumptions apply to living cells or the associated test conditions (Costa and Yin, 1999). Rather, cells are materially nonuniform, consisting of multiple families of structurally important and highly organized proteins that may exhibit a nonlinear behavior over finite deformations (e.g., see Janmey et al., 1991; Liu and Pollack, 2002). The goal of this work, therefore, is two-fold: to present a new nonlinear constitutive model for cells that accounts for their inherent material non-uniformity as well as potential material and geometric nonlinearities, and to extend a prior solution from the finite elasticity literature for use in a sub-class of AFM studies of cell mechanics. In particular, we submit that a constrained mixture model of the cytoskeleton offers potential advantages over many prior models for one can account for constituent-specific changes in mechanical properties that have been reported recently in AFM studies (e.g., Wu et al., 1998a; Rotsch and Radmacher, 2000).

Background

Constrained mixture models

Adherent cells consist of three primary components: the cell membrane, cytoplasm, and nucleus. Whereas a complete description of cell mechanics will require separate descriptions of the mechanical properties of each component, here we consider a homogenized idealization that holds away from the nucleus and in cases of negligible bending stiffness of the membrane. The cytoplasm consists of a viscous fluid (called the cytosol), distributed organelles, and the cytoskeleton. The cytoskeleton endows the cell with most of its structural integrity and consists of three primary constituents: actin filaments, intermediate filaments, and microtubules. These filaments are on the order of 5-25 nm in diameter and often distributed throughout the cytoplasm. Although one could employ a full mixture theory (cf. Rajagopal and Tao, 1995) to describe the mechanics of such a multi-constituent material, which would require solution of separate balance relations for the constituents, there is a lack of information on the interactions between the three primary constituents as well as between these constituents and the many accessory proteins (Alberts et al., 2002). Thus, it is not possible at present to postulate the constitutive relations for momentum exchanges between constituents that are needed in a full mixture theory. Following Humphrey (2002a), therefore, we adopt a homogenized rule-of-mixtures model for the stress response. This allows us to include the separate contributions of the primary cytoskeletal filaments and viscous cytosol without having to solve separate balance relations for each constituent, to quantify the momentum exchanges, or to prescribe partial traction boundary conditions. A general

rule of mixtures relation for the total Cauchy stress \mathbf{t} (subject to an overall linear momentum balance) can be written as $\mathbf{t} = \sum \phi^k \mathbf{t}^k$ where ϕ^k are individual mass fractions and \mathbf{t}^k the individual stress responses, whether elastic or viscous. Indeed, including both the “elastic” response of the filaments and the “viscous” response of the cytosol may allow one to model some of the complex viscoelastic responses exhibited by cells (e.g., see Heidemann et al., 1999).

For motivational purposes, let us also consider a simple case wherein any mechano-sensitive changes in the polymerization or depolymerization of the structural filaments occur in but a single altered (i.e., new) configuration. In this case, one must track constituents that existed prior to the perturbation in loading (original) plus those produced thereafter (new). Within the context of a rule-of-mixtures approach, the associated stress response can be written as (Humphrey, 2002a)

$$\begin{aligned} \mathbf{t} = & -p\mathbf{I} + \phi^c 2\tilde{\mu}\mathbf{D} + \phi_o^a \mathbf{t}^a(\mathbf{F}_{\kappa_o^a}) + \phi_o^i \mathbf{t}^i(\mathbf{F}_{\kappa_o^i}) + \phi_o^m \mathbf{t}^m(\mathbf{F}_{\kappa_o^m}) \\ & + \phi_n^a \mathbf{t}^a(\mathbf{F}_{\kappa_n^a}) + \phi_n^i \mathbf{t}^i(\mathbf{F}_{\kappa_n^i}) + \phi_n^m \mathbf{t}^m(\mathbf{F}_{\kappa_n^m}) \end{aligned} \quad (2.1)$$

where p is a Lagrange multiplier that enforces incompressibility over transient loading, \mathbf{D} is the stretching tensor (i.e., $2\mathbf{D} = \dot{\mathbf{F}}\mathbf{F}^{-1} + \mathbf{F}^{-T}\dot{\mathbf{F}}^T$ where the over-dot denotes a time-derivative), $\tilde{\mu}$ is a viscosity, the \mathbf{F}_κ ’s are deformation gradient tensors for each constituent relative to individual natural configurations κ_o (original) or κ_n (new), and the ϕ ’s are mass fractions (i.e., constituent mass per total mass) of individual constituents, which by definition are subject to the constraint

$$\phi^c + \phi_o^a + \phi_o^i + \phi_o^m + \phi_n^a + \phi_n^i + \phi_n^m = 1. \quad (2.2)$$

Specifically, the subscript o denotes “original” and n denotes “new” whereas the superscripts c , a , i , and m denote cytosol, actin, intermediate filaments, and microtubules, respectively. In other words, we assume that the stress response depends both on the response of extant constituents that formed prior to any perturbation in loading as well as on constituents that formed thereafter. (Note: although some constituents turnover continuously, there is no net change in mass fraction or mechanical behavior when they do so equally in an unchanging configuration, which we refer to as maintenance). In the absence of turnover in an altered configuration, the mass fractions of the new constituents are zero, thus yielding the standard rule-of-mixtures relation for stress.

Finally, note that the assumption of a constrained mixture requires that constituents deform together; because these constituents may have different natural (i.e., stress-free) configurations, the individual deformation gradients \mathbf{F}_k ’s need not be the same. Similarly, the individual stress responses \mathbf{t}^k are expected to differ ($k = a, i, m$ for actin, intermediate filaments, and microtubules, respectively). Indeed, this is one of the primary advantages of a mixture theory. Nevertheless, we emphasize that in such a formulation, the \mathbf{t}^k represent “constituent-dominated” phenomenological responses that implicitly include constituent-to-constituent interactions that cannot be quantified in sufficient detail (cf. Brodland and Gordon, 1990). See Humphrey (2002a) for more details on the basic theory.

Lessons from finite elasticity

It has been well known for nearly a century that biological soft tissues and elastomeric materials share many characteristic behaviors (see Treloar, 1975; Humphrey, 2002b). This similarity results, in large part, from both classes of materials exhibiting primarily an entropic, not energetic, elasticity due to their underlying long chain polymeric microstructures. Consequently, many results from finite (rubber) elasticity can be very useful in biomechanics. One solution that is particularly relevant to some AFM studies is that of a small, quasi-static indentation superimposed on a finite equibiaxial stretch of an initially isotropic, nonlinearly elastic, materially uniform, incompressible material whose behavior is described by a strain-energy function $W = W(I_1, I_2)$. Briefly, the associated constitutive relation for the Cauchy stress is

$$\mathbf{t} = -p\mathbf{I} + 2\frac{\partial W}{\partial I_1}\mathbf{B} - 2\frac{\partial W}{\partial I_2}\mathbf{B}^{-1} \quad (2.3)$$

where $\mathbf{B} = \mathbf{F}\mathbf{F}^T$ is the left Cauchy-Green tensor and $I_1 = \text{tr}\mathbf{C}$ and $2I_2 = (\text{tr}\mathbf{C})^2 - \text{tr}\mathbf{C}^2$ are the principal invariants of the right Cauchy-Green tensor $\mathbf{C} = \mathbf{F}^T\mathbf{F}$. For an initial, finite equibiaxial stretch, we let $\mathbf{F} = \text{diag}[\mu, \mu, \lambda]$ where μ is the in-plane stretch and λ the out-of-plane stretch; by incompressibility, $\lambda = 1/\mu^2$ thus allowing the deformation to be parameterized by one stretch. For completeness, let us summarize past results for the small, superimposed indentation.

The superimposed indentation force-depth (P - δ) relationship was found by Green et al. (1952) and Beatty and Usmani (1975). It can be written as

$$P = 2\pi \frac{\Gamma(W)}{\Sigma(W)} \hat{f}(\delta) \quad (2.4)$$

where $\Gamma(W)$ and $\Sigma(W)$ are functionals that depend on the strain-energy function W and the finite equibiaxial stretch μ whereas the function $\hat{f}(\delta)$ depends on the geometry of the tip of the rigid indenter. For example, Costa and Yin (1999) list the following results for different tip geometries. For a flat-ended circular indenter of radius a ,

$$\hat{f}(\delta) = \frac{2a\delta}{\pi}; \quad (2.5)$$

for a spherical tip of radius a ,

$$\hat{f}(\delta) = \frac{4}{3\pi} \sqrt{a\delta^3}; \quad (2.6)$$

for a conical tip with tip angle 2Φ ,

$$\hat{f}(\delta) = \frac{2 \tan \Phi}{\pi^2} \delta^2; \quad (2.7)$$

and for a blunted cone-shaped tip of angle 2Φ , which transitions at radius b to a spherical cap of radius a ,

$$\hat{f}(\delta) = \frac{2}{\pi} \left[r_c \delta - \frac{r_c^2}{2 \tan \Phi} \left(\frac{\pi}{2} - \arcsin \left(\frac{b}{r_c} \right) \right) - \frac{r_c^3}{3a} + (r_c^2 - b^2)^{1/2} \left(\frac{b}{2 \tan \Phi} + \frac{r_c^2 - b^2}{3a} \right) \right], \quad (2.8)$$

where the radius of contact, $r_c \geq b$, and is obtained from Eq. (2.9), namely (Briscoe et al., 1994)

$$\delta + \frac{r_c}{a} \left[(r_c^2 - b^2)^{1/2} - r_c \right] - \frac{r_c}{\tan \Phi} \left[\frac{\pi}{2} - \arcsin \left(\frac{b}{r_c} \right) \right] = 0. \quad (2.9)$$

Finally, Humphrey et al. (1991) list the following results for computing $\Gamma(W)$ and $\Sigma(W)$:

$$\Gamma = \frac{(A + K_1 B)\sqrt{K_1}}{1 + K_1} - \frac{(A + K_2 B)\sqrt{K_2}}{1 + K_2}, \quad \text{and} \quad \Sigma = \frac{K_1}{1 + K_1} - \frac{K_2}{1 + K_2}, \quad (2.10)$$

where

$$A = 2\lambda^2(W_1 + \mu^2 W_2), \quad B = 2\mu^2(W_1 + \mu^2 W_2) \quad (2.11)$$

and K_1 and K_2 (dimensionless) are determined by solving the following quadratic equation for K :

$$BK^2 + (A + B - C - D)K + A = 0 \quad (2.12)$$

with,

$$C = 4\mu^2 \left[(W_1 + \mu^2 W_2) + (\mu^2 - \lambda^2)(W_{11} + W_{22}\mu^2(\mu^2 + \lambda^2) + W_{12}(2\mu^2 + \lambda^2)) \right] \quad (2.13)$$

and

$$D = 4\lambda^2 \left[(W_1 + \mu^2 W_2) + (\lambda^2 - \mu^2)(W_{11} + 2W_{22}\mu^4 + 3W_{12}\mu^2) \right]. \quad (2.14)$$

Note that, for convenience, we denote

$$W_i \equiv \frac{\partial W}{\partial I_i}, \quad W_{ij} \equiv \frac{\partial^2 W}{\partial I_i \partial I_j}, \quad i, j = 1, 2. \quad (2.15)$$

Together, Eqs. (2.4)-(2.15) allow one to compute the indentation force-depth relation for an incompressible, initially isotropic material that is first stretched equibiaxially (note: this stretch induces an anisotropy relative to the original reference configuration). In the next section, we extend this result for a special case of a new relationship for cell

mechanics that accounts for the separate contributions of the three primary cytoskeletal constituents.

New theoretical framework

A constitutive relation for cells

Many different models have been proposed for the constitutive behavior of cells (e.g., see Humphrey, 2002a; Stamenovic and Ingber, 2002). These include tensegrity models, percolation models, soft glassy rheological models, mixture models, and classical models based on linearized elasticity or viscoelasticity. Notwithstanding the potential advantages of the different models, we submit that constrained rule-of-mixture models (cf. Eq. 2.1) allow one to include nonlinear elasticity and viscoelasticity, different properties and distributions of individual constituents, and most importantly the different rates and extents of turnover of individual constituents. Here, therefore, consider the following relation for the Cauchy stress,

$$\mathbf{t} = -p\mathbf{I} + 2\mathbf{F}\frac{\partial W}{\partial \mathbf{C}}\mathbf{F}^T + \phi^c 2\tilde{\mu}(\phi^c)\mathbf{D}, \quad (2.16)$$

where the viscosity may depend on the volume fraction of the cytosol. That is, as insoluble constituents are depolymerized, their fragments may alter the viscosity (cf. Herant et al., 2003). More important here, however, we borrow from the work of Lanir (1983) to construct a strain-energy function for a potentially evolving cytoskeleton, while emphasizing that the resulting relations are microstructurally-motivated, but phenomenological, namely

$$W = \sum_{k=1}^N \int_0^{2\pi} \int_{-\pi/2}^{\pi/2} \phi^k R^k(\varphi, \theta) w^k(\alpha^k) \cos \varphi d\varphi d\theta, \quad (2.17)$$

where $w^k(\alpha^k)$ is a 1-D strain energy function for a filament and α^k is its stretch; the superscript k can denote a particular constituent as well as its natural configuration (e.g., original versus new). The function $R^k(\varphi, \theta)$ represents the original distribution of orientations of a filament family k and ϕ^k are mass fractions. Consequently,

$$\frac{\partial W}{\partial C_{MN}} = \sum_{k=1}^N \int_0^{2\pi} \int_{-\pi/2}^{\pi/2} \phi^k R^k(\varphi, \theta) \frac{\partial w^k}{\partial \alpha^k} \frac{\partial \alpha^k}{\partial C'_{11}} \frac{\partial C'_{11}}{\partial C_{MN}} \cos \varphi d\varphi d\theta, \quad (2.18)$$

where the 1' (i.e., primed) coordinate axis coincides with the direction of a generic filament (Fig. 2.2), and C'_{11} is obtained from a tensorial transformation of C_{MN} . This relation will prove useful below. Hence, we have

$$t_{ij} = -p\delta_{ij} + 2 \sum_{k=1}^N \phi^k \left(\int_0^{2\pi} \int_{-\pi/2}^{\pi/2} R^k(\varphi, \theta) \frac{\partial w^k}{\partial \alpha^k} \frac{1}{2\alpha^k} \frac{\partial C'_{11}}{\partial C_{MN}} \cos \varphi d\varphi d\theta \right) F_{iM} F_{jN} + \phi^c 2\tilde{\mu}(\phi^c) D_{ij} \quad (2.19)$$

Clearly then, in the absence of constituent turnover, our constitutive relation can be written as a simple rule-of-mixtures with each primary constituent having a single reference configuration (i.e., $N = 1, 2, 3$ for original actin a , intermediate filaments i , and microtubules m), namely

$$\mathbf{t} = -p\mathbf{I} + \phi^a \mathbf{t}^a + \phi^i \mathbf{t}^i + \phi^m \mathbf{t}^m + \phi^c 2\tilde{\mu}(\phi^c) \mathbf{D}. \quad (2.20)$$

Turnover of constituents can easily be incorporated in Eq. (2.19), in principle, given appropriate kinetics for the mass fractions, information on the potential evolution of the individual natural configurations, and information on the potential evolution of the distribution of the filaments. This is left for subsequent consideration.

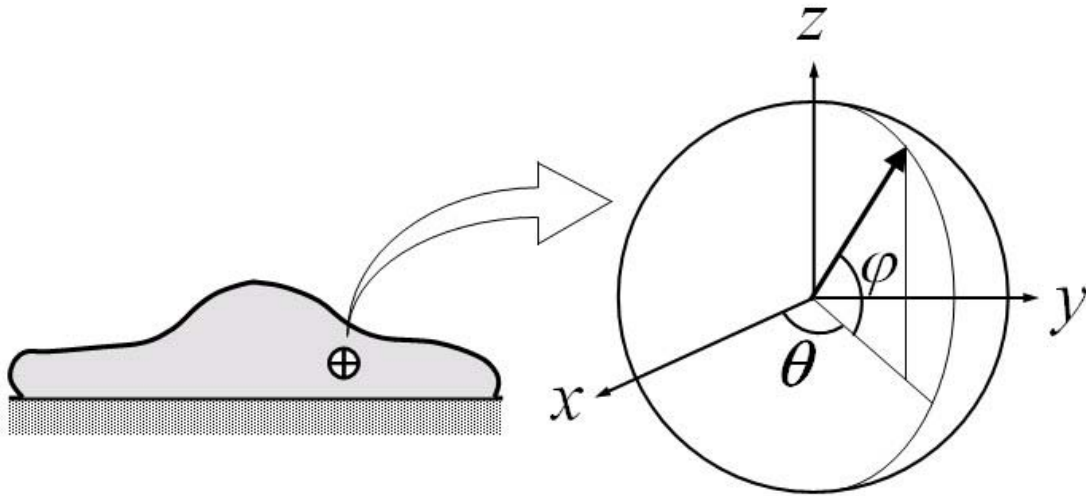


Fig. 2.2. Local spherical coordinate system used for microstructurally-motivated, phenomenological constitutive relations of a living cell. The arrow represents the orientation of an individual filament belonging to any of the three primary families of cytoskeletal filaments. The function $R^k(\varphi, \theta)$ quantifies the distribution of all such orientations.

Small indentation superimposed on a finite equibiaxial stretch

Conceptually, it may be prudent to think of at least four configurations for the cell in an AFM test (Fig. 2.3). First, we have a non-adherent cell with perhaps a fairly random distribution of cytoskeletal filaments. Deposition of the cell onto a substrate involves two phases: initial contact, with an upregulation of integrins, followed by an active spreading. Relative to the non-adherent reference configuration, we might think of this spreading as somewhat of an in-plane stretch. Finally, if the substrate is deformable, the cell could be stretched further prior to testing with the AFM. This potential sequence of events motivates the consideration of a small indentation superimposed on a large “in-plane” deformation of a mixture that originally had a nearly uniform distribution of con-

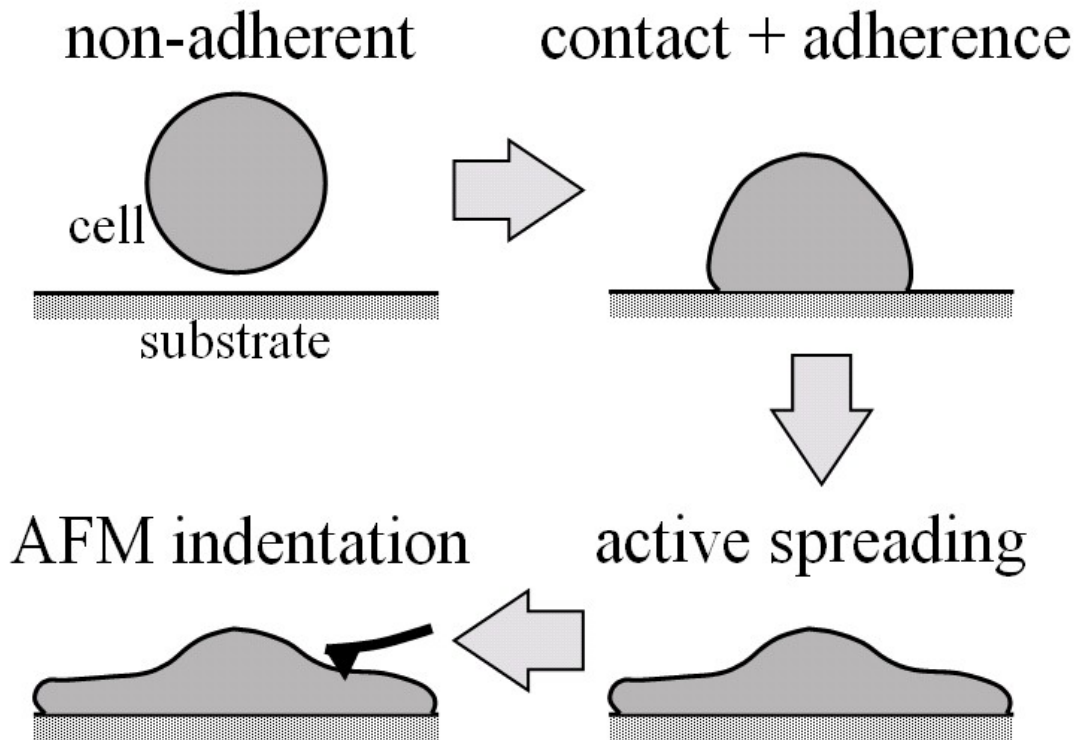


Fig. 2.3. Four configurations for an adherent cell, including an assumed materially isotropic cell in a non-adherent, traction-free reference configuration. Adherence and active spreading likely change the material symmetry from isotropic to anisotropic via an affine deformation-dependent mechanism and possibly active remodeling (not considered explicitly).

stituents. Whereas the aforementioned solution for the relation P - δ (Eq. 2.4) was derived for a 3-D stored energy function $W(I_1, I_2)$, the proposed strain-energy for the cell (Eq. 2.17) is written in terms of individual 1-D stored energy functions w^k that depend solely on the stretch α^k experienced by the individual constituent. Fortunately, these stretches relate to the macroscopic deformation \mathbf{C} if we assume affine deformations. Hence, we merely need transformation relations between derivatives with respect to the invariants I_i

and those in terms of the components of \mathbf{C} in order to utilize prior results for the indentation solution. Note, therefore, that

$$\frac{\partial W}{\partial C_{MN}} = \frac{\partial W}{\partial I_1} \frac{\partial I_1}{\partial C_{MN}} + \frac{\partial W}{\partial I_2} \frac{\partial I_2}{\partial C_{MN}} \quad (2.21)$$

whereby for an in-plane equibiaxial stretch, we need only consider derivatives with respect to C_{11} , C_{22} , and C_{33} . These provide three equations in terms of the two “unknown” derivatives of W with respect to I_1 and I_2 , which are denoted by W_1 and W_2 , respectively. For an equibiaxial stretch, however, the results for the in-plane components C_{11} and C_{22} are the same and it is easy to show that

$$\begin{aligned} W_1 &= \frac{1}{C_{11} - C_{33}} \left((C_{11} + C_{22}) \frac{\partial W}{\partial C_{11}} - (C_{22} + C_{33}) \frac{\partial W}{\partial C_{33}} \right) \\ &= \frac{1}{\mu^2 - \lambda^2} \left(2\mu^2 \frac{\partial W}{\partial C_{11}} - (\mu^2 + \lambda^2) \frac{\partial W}{\partial C_{33}} \right) \end{aligned} \quad (2.22)$$

$$W_2 = \frac{1}{C_{33} - C_{11}} \left(\frac{\partial W}{\partial C_{11}} - \frac{\partial W}{\partial C_{33}} \right) = \frac{1}{\lambda^2 - \mu^2} \left(\frac{\partial W}{\partial C_{11}} - \frac{\partial W}{\partial C_{33}} \right). \quad (2.23)$$

Next, let $W_1 = \hat{g}(C_{11}, C_{22}, C_{33})$ and $W_2 = \tilde{g}(C_{11}, C_{22}, C_{33})$ and consider the following derivatives:

$$\frac{\partial \hat{g}}{\partial C_{MN}} = \frac{\partial \hat{g}}{\partial I_1} \frac{\partial I_1}{\partial C_{MN}} + \frac{\partial \hat{g}}{\partial I_2} \frac{\partial I_2}{\partial C_{MN}}, \quad \frac{\partial \tilde{g}}{\partial C_{MN}} = \frac{\partial \tilde{g}}{\partial I_1} \frac{\partial I_1}{\partial C_{MN}} + \frac{\partial \tilde{g}}{\partial I_2} \frac{\partial I_2}{\partial C_{MN}}, \quad (2.24)$$

which provide six equations in terms of the four “unknown” second derivatives of W with respect to the invariants, which we denote by $W_{ij} = W_{ji}$ (cf. Eq. 2.15). As before, however, the equations for the components C_{11} and C_{22} provide the same information,

thus leaving four equations. Solving these four equations for the four second derivatives of W with respect to the principal invariants of \mathbf{C} yields,

$$W_{11} = \frac{1}{(C_{11} - C_{33})^2} \left[\begin{aligned} &(C_{11} + C_{22})^2 \frac{\partial^2 W}{\partial C_{11}^2} - 2(C_{11} + C_{22})(C_{22} + C_{33}) \frac{\partial^2 W}{\partial C_{11} \partial C_{33}} + \\ &(C_{22} + C_{33})^2 \frac{\partial^2 W}{\partial C_{33}^2} + \frac{2(C_{11} + C_{22})(C_{22} + C_{33})}{C_{11} - C_{33}} \left(\frac{\partial W}{\partial C_{33}} - \frac{\partial W}{\partial C_{11}} \right) \end{aligned} \right], \quad (2.25)$$

$$W_{12} = \frac{1}{(C_{11} - C_{33})^2} \left[\begin{aligned} &(C_{11} + C_{22}) \left(\frac{\partial^2 W}{\partial C_{33} \partial C_{11}} - \frac{\partial^2 W}{\partial C_{11}^2} \right) + (C_{22} + C_{33}) \left(\frac{\partial^2 W}{\partial C_{11} \partial C_{33}} - \frac{\partial^2 W}{\partial C_{33}^2} \right) \\ &+ \frac{(C_{11} + 2C_{22} + C_{33})}{C_{11} - C_{33}} \left(\frac{\partial W}{\partial C_{11}} - \frac{\partial W}{\partial C_{33}} \right) \end{aligned} \right], \quad (2.26)$$

where $W_{12} = W_{21}$, and

$$W_{22} = \frac{1}{(C_{11} - C_{33})^2} \left[\frac{\partial^2 W}{\partial C_{11}^2} - 2 \frac{\partial^2 W}{\partial C_{11} \partial C_{33}} + \frac{\partial^2 W}{\partial C_{33}^2} + \frac{2}{C_{33} - C_{11}} \left(\frac{\partial W}{\partial C_{11}} - \frac{\partial W}{\partial C_{33}} \right) \right]. \quad (2.27)$$

Recall that $\mathbf{C} = \text{diag}[\mu^2, \mu^2, \lambda^2]$ for our case herein, with $\lambda = 1/\mu^2$, which allows these equations to be specialized. Most importantly, however, we can now compute A , B , C and D in Eqs. (2.11)-(2.14), and thus compute $\Gamma(W)/\Sigma(W)$ in Eq. (2.10) – this allows us to compute indentation force-depth relations P - δ for the model cell (Eqs. 2.16-2.20). Although the final equation can be written directly, it proves expedient to calculate numerically the requisite quantities from these simple formulae¹.

Finally, because little is yet known about the specific functional forms of $w^k(\alpha^k)$ for the individual constituents of the cytoskeleton, or the associated values of

¹ Explicit derivations were carried out for a Mooney-Rivlin material whereby the classical result was confirmed (cf. equation 8 in Humphrey et al. 1991).

the material parameters, we nondimensionalize the problem to allow illustrative simulations. Let length, time, and mass scales be, respectively,

$$L_s = d, \quad T_s = \sqrt{\frac{\rho d^2}{E}}, \quad M_s = \rho d^3, \quad (2.28)$$

where d is the diameter of the cell in the non-adherent state (see Fig. 2.3), ρ is the overall mass density of the cell, and

$$E = \lim_{\mu \rightarrow 1} \left(\frac{\Gamma}{\Sigma} \right), \quad (2.29)$$

where E is an initial overall elastic modulus of a cell that can be estimated at $\mu = \lambda = 1$, with Γ and Σ obtained from Eq. (2.10). Consequently, Eq. 2.4 can be written as

$$\Psi = 2\pi \Theta \eta(x), \quad (2.30)$$

where

$$\Psi = \frac{P}{d^2 E}, \quad \Theta = \frac{\Gamma/\Sigma}{E}, \quad \eta = \frac{\hat{f}(\delta)}{d^2}, \quad (2.31)$$

and $x = \delta/d$.

Illustrative simulations

There is a pressing need for data that are sufficient for identifying specific forms of the constitutive functions (including $w^k(\alpha^k)$ and $R^k(\varphi, \theta)$) and calculating values of the associated material parameters for each constituent. Such data often have to await the development of a theoretical framework, however, for without a framework one often does not know what to measure (e.g., overall modulus in a Hertz model versus stiffness

and orientation for individual filaments). Notwithstanding the current lack of sufficient data, let us illustrate qualitatively some predictions of the present theoretical framework. Such simulations help us to develop intuition and indeed may help us to interpret future experimental results.

Illustrative mechanical behaviors

Despite scant information on the mechanical behavior of individual filaments (or, more precisely, filament-dominated behaviors that include the effects of select accessory proteins), it appears that these behaviors may be qualitatively similar to those of soft tissue – nonlinear with slight hysteresis (Janmey, 1991; Liu and Pollack, 2002). Hence, one possible form for the 1-D energy function is (Humphrey and Yin, 1987)

$$w^k(\alpha^k) = \frac{1}{2} c^k \left[\exp(c_1^k (\alpha^k - 1)^2) - 1 \right], \quad (2.32)$$

where c^k and c_1^k are separate material parameters for each family of constituents k .

Another possible form is (Lanir, 1983)

$$w^k(\alpha^k) = \frac{1}{2} c_2^k (\alpha^k - 1)^2, \quad (2.33)$$

which yields a linear first Piola-Kirchhoff stress vs. stretch relation (note: Eq. 2.32 reduces to Eq. 2.33 in the limit as $\alpha^k \rightarrow 1$, with $c_2^k \cong c^k c_1^k$, no sum on k).

Similarly, despite increasing data from confocal and multi-photon microscopy, there is little information on specific distributions of the orientations of the cytoskeletal filaments. For purposes of illustration, however, consider a three-dimensional von Mises

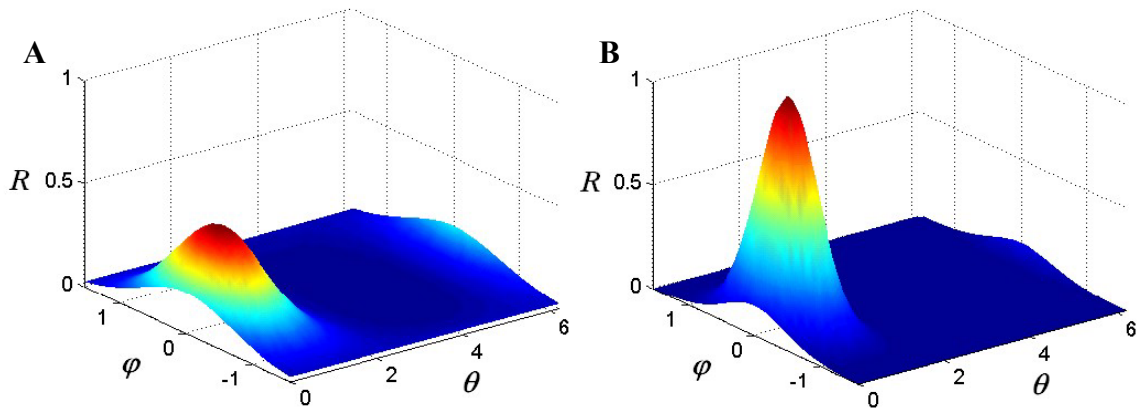


Fig. 2.4. Illustrative (possible) distributions of cytoskeletal filaments given by a von Mises-Fisher distribution function (cf. Eq. 2.34). (A) $\kappa = 3$, $\beta = 0$, $\gamma = \pi/4$, (B) $\kappa = 7$, $\beta = 0$, $\gamma = \pi/4$.

-Fisher distribution that results directly by generalizing the von Mises distributions on the two-dimensional circle (Fisher et al., 1987), namely

$$R^k(\varphi, \theta) = \frac{\kappa}{4\pi \sinh \kappa} \left[\exp \kappa (\cos \varphi \cos \beta \cos(\theta - \gamma) + \sin \varphi \sin \beta) \right]; \quad (2.34)$$

$$(-\pi/2 \leq \varphi \leq \pi/2, 0 \leq \theta \leq 2\pi).$$

This distribution has three parameters: κ , β , and γ . κ is a shape, or concentration factor. The larger the value of κ the more the distribution is concentrated towards the direction (β, γ) – see Fig. 2.4. β and γ are location parameters where the distribution has rotational symmetry about the direction (β, γ) . Since R^k is a probability density function, its integral over all possible orientations must satisfy the normalization condition,

$$\int_0^{2\pi} \int_{-\pi/2}^{\pi/2} R^k(\varphi, \theta) \cos \varphi d\varphi d\theta = 1 \quad \forall k. \quad (2.35)$$

Illustrative numerical results

Recalling Fig. 2.3, let us assume that each family of filaments is randomly distributed in the non-adherent reference configuration. That is, let us assume an initial isotropy despite any stretch-induced anisotropy associated with cell spreading or subsequent stretching of the substrate. (note: such stretch-induced changes in orientation can be calculated simply given $\alpha^k \mathbf{m}^k = \mathbf{F}_{\kappa^k}^k \mathbf{M}^k$ where \mathbf{M}^k and \mathbf{m}^k are unit vectors in the direction of a particular filament in original and deformed configurations, respectively). Consequently, let $R^k(\varphi, \theta) = 1/4\pi$. Let volume fraction of the actin filaments be $\phi^a = 0.038$ (Cheng et al., 2000). Material parameters for each filament within the cytoskeleton are chosen such that the actin filaments are stiffer in extension than the microtubules, with the intermediate filaments exhibiting an intermediate extensional stiffness (Janmey et al., 1991). Given such values, we can estimate the volume fractions of the microtubules and intermediate filaments. Assuming that their volume fractions are the same, and using empirical results from Rotsch and Radmacher (2000), which show that the “elastic modulus” of the cell decreases by a factor of 3 when actin filaments are disrupted, we compare the initial elastic moduli E of two cases, control and actin-disrupted (Eq. 2.29). Of course, if the filament is disrupted completely, its volume fraction ϕ^k is zero. The parameters for our calculations are given in Table 2.1. Finally, for purposes of non-dimensionalization, note that the volume of an average culture cell is approximately 4 picoliters (Alberts et al., 2002), thus let $d = 20$

Table 2.1
Material parameters for a model cell

Nondimensional Parameter	Actin Filaments	Microtubules	Intermediate Filaments
Volume Fraction ϕ	0.038	0.017	0.017
Stiffness Parameter c/E	1.78	1.78	1.78
Material Parameter c_1	120	50	80
Stiffness Parameter c_2/E	214	89	142

Note: the volume fraction for actin was taken from Cheng et al., (2000). The volume fractions of the microtubules and intermediate filaments were estimated from Eqs. 2.10-2.15, 2.29, and from the experiments of Rotsch and Radmacher (2000). Stiffness parameters and material parameters were assumed based on Janmey (1991); that for c_2/E was selected for direct comparisons between the exponential and linear models.

μm . Furthermore, let $\rho = 1$ g/ml for water is the most abundant substance in cells (Alberts et al. 2002).

Assuming a quasi-static indentation (i.e., $\mathbf{D} = \mathbf{0}$ in Eq. 2.16), consider P - δ (actually $\Psi - \eta$) results for different values of the in-plane stretch $\mu \in [1, 1.12]$ for both an exponential and a linear behavior (Eqs. 2.32 and 2.33) of the filaments and with a flat-ended cylindrical indenter (Fig. 2.5). Similarly, consider results at a single stretch ($\mu = 1.2$) for exponential-type filament behaviors with four different indenter tips (Fig. 2.6A). If we interpret the slope of the force-depth relation as a measure of the “stiffness” of the cell, we see that both the degree of finite stretch (e.g., degree of spreading) and the geometry of the tip dramatically affect this result given the same material properties. In particular, only the flat-ended tip yields a linear force-depth relation for the small indentation. The non-flat tipped indenters contact increasingly more material as they indent deeper. Finally, note that removal of individual constituents reduces the stiffness as expected (Fig. 2.6B): disruption of the actin filaments can red-

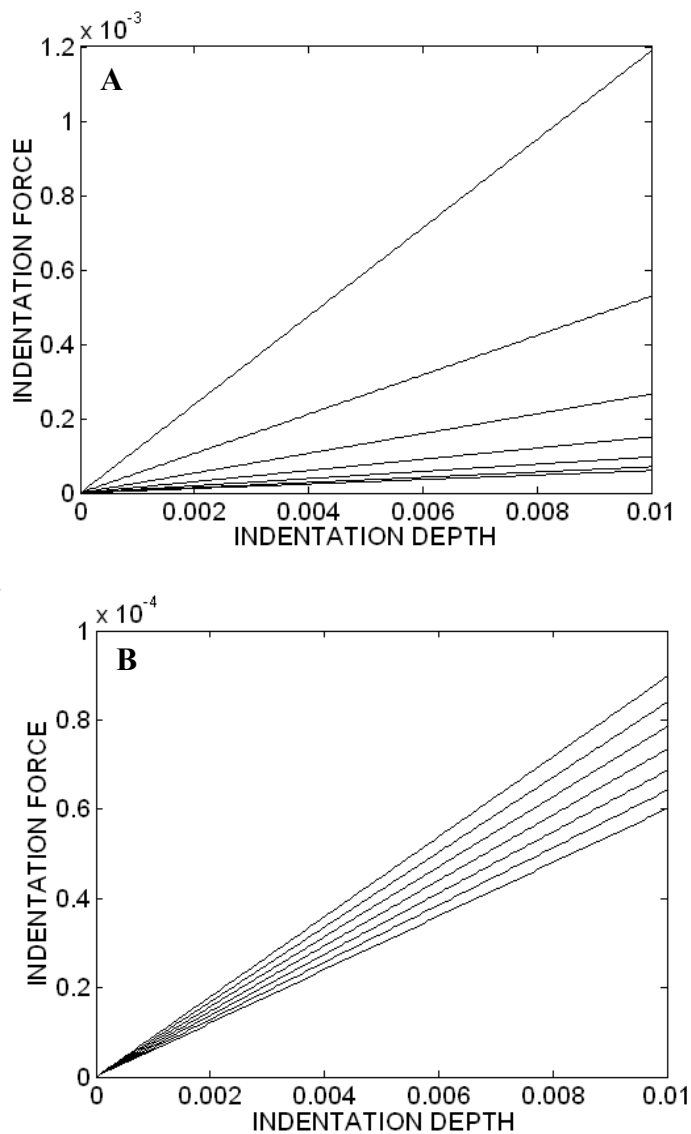


Fig. 2.5. Combined out-of-plane indentation and in-plane equibiaxial stretch for (A) exponential-type filaments and (B) linear-type filaments, each indented by a flat-ended circular cylinder with radius 30 nm. Each line corresponds to different in-plane stretches, from lower to upper, of $\mu = 1.00$ to 1.12 in steps of 0.02. All results are non-dimensional to emphasize the qualitative responses, not the specific values.

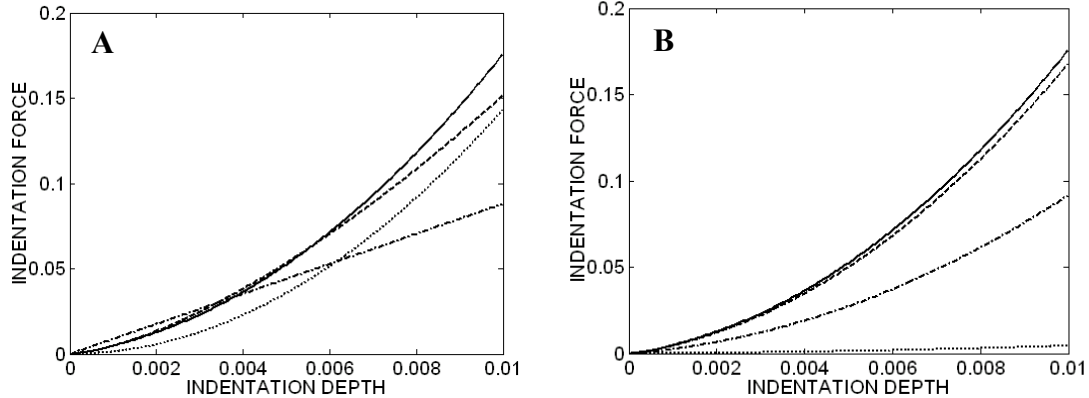


Fig. 2.6. Combined indentation and equibiaxial in-plane stretch, $\mu = 1.2$, for the exponential-type filament behavior. (A) Effects of four different indenter tips: flat-ended circular cylinder with radius $a = 30$ nm (dash-dotted line, which is linear), sphere with radius $a = 30$ nm (dashed line), cone with tip angle $2\Phi = 75^\circ$ (dotted line), and blunted cone with tip angle $2\Phi = 75^\circ$ and radius $a = 30$ nm (solid line). The nonlinear responses (for all but the flat-ended indenter) are due, in part, to the nonlinearly increasing contact area between the indenter and cell. (B) Effects of cytoskeleton disrupting drugs with blunted cone, with $2\Phi = 75^\circ$ and $a = 30$ nm: control (solid line), actin filament disrupting drugs (dotted line for disruption of all actin filaments, and dash-dotted line disruption of half the actin filaments), and microtubule and intermediate filament disrupting drugs (dashed line). We assume that if the filament is disrupted completely, the volume fraction ϕ of the corresponding filament is zero. Note that the predicted behavior is dominated by the actin. All results are non-dimensional to emphasize the qualitative responses, not the specific values.

-uce the stiffness substantially, whereas there can be little contribution to the overall cytoskeletal stiffness by the microtubules or intermediate filaments. This observation agrees with the empirical findings of Wakatsuki et al. (2000) and Wu et al. (1998a). Although not shown, additional simulations with different values of the material parameters (cf. Table 2.1) revealed qualitatively similar results: decreasing the stiffness of the actin dramatically decreased the indentation force at a given indentation depth and

tip-geometry whereas uniformly raising or lowering the values of the parameters had no effect due to the non-dimensionalization.

Discussion

Many different experimental methods exist for interrogating the biomechanical properties and mechanobiological responses of cells. They include: atomic force microscopy, magnetic bead cytometry, micro-fabricated cantilevers, micro-patterned surfaces, micro-pipet aspiration, optical traps, stretching of cells on flexible membranes, laminar flow chambers, and rotating bioreactors. Each method promises new insight into the wonderfully complex structure, function, and properties of living cells, and each warrants rigorous biomechanical analysis. Herein, we focused on atomic force microscopy not only because of its widespread usage, but primarily because of the need for improved methods of data analysis.

Many investigators recognize that the simplifying assumptions inherent to the Hertz solution do not apply in most AFM studies on cells. This was shown convincingly via finite element simulations by Costa and Yin (1999) – they wrote, “Widely applied infinitesimal strain models agreed with FEM results for linear elastic materials, but yielded substantial errors in the estimated properties for nonlinear elastic materials.” Consequently, some employ nonlinear empirical P - δ relations and then try to ascribe meaning to the associated parameters (e.g., Miyazaki and Hayashi, 1999; Sato et al., 2000). This approach is limited, however, by the inability to separate structural from material stiffnesses; indeed, it has no biomechanical basis. Alternatively, others appear

to rationalize using the Hertz solution by arguing that measuring absolute values of the material properties is less important than delineating relative changes from cell-to-cell or intervention-to-intervention. Finally, some appear to use the Hertz solution simply because of a lack of a viable alternative. Mathur et al. (2001) imply, for example, that there is simply a need for further development of applicable theoretical frameworks. Regardless, there is a pressing need to move beyond the assumptions of a linearly elastic behavior of a single constituent continuum under infinitesimal strains.

The approach and findings of Costa and Yin (1999) represent a pivotal step in improving analyses of AFM experiments. Nonetheless, their finite element solutions are limited largely because of the use of a commercially available code that is best suited for strain-energy functions $W = \hat{W}(I_1, I_2)$ that describe the isotropic behavior of single constituent (i.e., materially uniform) continua. Cells, in contrast, contain multiple structurally important constituents that are able to remodel individually to different extents and at different rates. Indeed, recent advances in molecular biology that allow one to selectively modify individual constituents (e.g., see Wu et al., 1998a; Rotsch and Radmacher, 2000) necessitate a more general theoretical framework for analysis. Albeit based on a number of simplifying assumptions – e.g., small, quasi-static indentations on equibiaxially stretched cells – the approach presented herein can account for the separate orientations, properties, and deformations of multiple constituents within the cytoskeleton, and thus changes in the mechanical response of cells that are induced by biological or mechanical stimuli such as applying cytoskeleton disrupting drugs or pre-stretch. Indeed, despite the need to introduce particular constitutive relations to

numerically illustrate the theory, these can be varied easily as demanded by increasingly better data, thus rendering the overall theory more general.

We emphasize that the two primary uses of such a framework should be to guide experimentation (e.g., highlight what needs to be measured, such as constituent properties, orientations, and mass fractions) and to serve as a check for future finite element analyses of AFM, which will be needed to study additional classes of tests. In particular, the present results cannot be used in cases wherein the indentation is above the nucleus or near the periphery where the effects of the underlying substrate are pronounced. In such cases, finite element analyses will be essential. Likewise, the present results should only be used in tests wherein the indentation is “small” and “quasi-static”. This reminds us again that theory should guide experiment. Finally, the most basic issue is that of the continuum assumption. The dimensions of the cell are on the order of μm whereas those of the cytoskeletal filaments are on the order of nm, which suggest that a continuum assumption may be reasonable as used in most papers to date². Nevertheless, the diameter of the indenter is often on the order of 10-50 nm, similar to that of the diameters of the primary constituents, thus this merits careful attention. This could be addressed, in part, by comparing predictions with additional experiments and would likely be aided by simultaneous imaging of the cytoskeleton. Conversely, one may need to consider larger diameter indenters, particularly ones that are flat-ended for they alone can yield linear force-depth data. Of course, in the final analysis, as noted by Truesdell and Noll (1965), “Whether the continuum approach is

² Other characteristic length scales for the structure could include pore size, inter-filament distances, and so on.

justified, in any particular case, is a matter, not for the philosophy or methodology of science, but for the experimental test.” Each case must be so justified, depending on the particular test and its overall goal. Going beyond a continuum approach will, of course, require remarkably fine detail on the distributions and interactions of all constituents, a significant challenge.

In conclusion, the complex structure and properties of living cells demands continued research into improved models. At the minimum, we should account for the nonlinear material behavior over finite strains of a multi-constituent material. The present work describes one step toward that goal, one that synthesizes prior work on microstructural models of soft tissues and an analytical solution from finite elasticity. It is hoped that this new model allows improved interpretation of sub-classes of AFM tests and, more importantly, that it provides some direction for further research.

CHAPTER III

TIME-DEPENDENT CHANGES IN CELL STIFFNESS AND FOCAL ADHESION AREA IN RESPONSE TO CYCLIC STRETCH

Introduction

Mechanical forces are critical in the development and continual remodeling of most tissues. Amongst other stimuli, abnormal strain profiles have been implicated in the pathogenesis of a number of diseases affecting arteries, particularly atherosclerosis (Thubrikar, 1988), and pressure overload causes cardiovascular hypertrophy (Collins et al., 1996). At the cellular level, strain transferred via the extracellular matrix has been shown to elicit numerous responses such as signal transduction and altered gene expression, which in turn alters cell migration, proliferation, adhesion, and cytoskeletal reorganization (Sumpio et al., 1987; Reusch et al., 1996; Smith et al., 1997; Kim et al., 1999; Li and Xu, 2000; Goldschmidt et al., 2001). Of particular interest here, numerous reports demonstrate cytoskeletal rearrangement in response to substrate deformation (Costa et al., 2002; Hayakawa et al., 2001; Smith et al., 1997; Takemasa et al., 1998; Wang et al., 2000, 2001; Yoshigi et al., 2003). For example, Smith et al. (1997) compared unstretched and cyclically stretched cells by transmission electron microscopy and fluorescence microscopy and suggested that cyclic stretching increases the number and organization of actin filaments (F-actin) and focal adhesions (FA) compared to the unstretched situation. Cunningham et al. (2002) used standard western blotting techniques to quantify focal contact associated proteins in smooth muscle cells subjected

to cyclic strain and suggested that insoluble levels of focal contact components are altered rapidly following the application of an appropriate number of mechanical perturbations. These two ideas, that mechanical strain induces F-actin polymerization and increases FA assembly, imply that the increased formation and reorganization of cytoskeletal filaments in the cells subjected to perturbations may be a consequence of FA changes.

It is generally accepted that the cytoskeleton is the major determinant of cell stiffness (Wu et al., 1998a; Smith et al., 2003; Huang et al., 2005). Relationships between cytoskeletal remodeling and the mechanical properties of cells have been studied extensively given the recent development of techniques capable of probing and manipulating forces and displacements less than a piconewton and a nanometer, respectively (for a review, see Vliet et al., 2003; Huang et al., 2004). Nonetheless, little is known about the quantitative relationship between the mechanical properties of cells and cytoskeletal remodeling.

In this study, we developed a simple cell extension device that can be combined with atomic force microscopy (AFM) and confocal microscopy to examine the time course of changes in cell stiffness and cytoskeletal remodeling, respectively. Rapid changes, within a few minutes, in cell stiffness were observed following cyclic strain for up to 60 minutes. The time course of changes in cytoskeletal remodeling, obtained from immunofluorescence micrographs, was consistent with the changes in cell stiffness.

Materials and methods

Design of cell extension device

Design criteria for the cell stretching device were: (a) homogeneous, equi-biaxial strain field throughout the membrane, (b) stationary plane of focus allowing cell observation during cyclic stretching, (c) chamber design for growing and stimulating living cells in an aqueous environment, and (d) real time stiffness measurement following stretching on an atomic force microscope stage.

The device applies a cyclic, uniform equibiaxial stretch to a silicone elastic membrane by dynamic infusion and withdrawal of air using a programmable syringe pump (Model 44, Harvard Apparatus, South Natick, MA) (Fig. 3.1). The device consists of a channeled polycarbonate cylinder that serves as the wall of the cell culture chamber, a transparent silicone elastic membrane (0.127 mm in thickness, Specialty Manufacturing Inc., Saginaw, MI), and a polycarbonate holder ring that clamps the membrane. The membrane serves as the growth surface for cells and remains in the same plane during stretching. The channeled ring has smooth rounded edges at the point of contact with the membrane substrate to reduce friction during stretching. The device permits in situ visualization of cell geometry and deformation via an elastic membrane that is transparent and accessible to the objective of an inverted microscope. The overall dimensions of the device are 5.3 cm in diameter and 1.6 cm in height, which allows it to be secured on the stage of an AFM using a magnetic ring that holds the device in place.

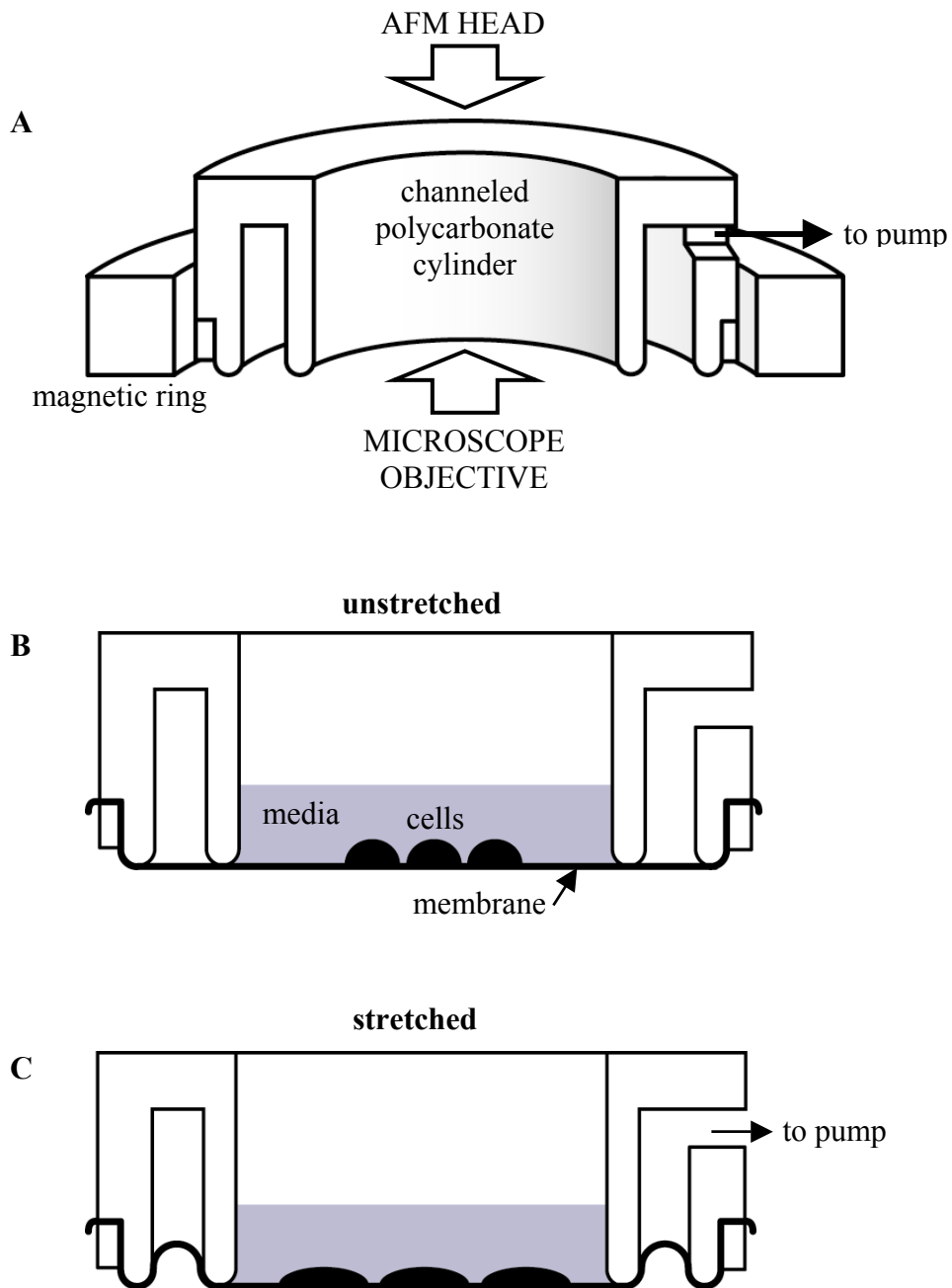


Fig. 3.1. Schema of the cell extension device. The device consists of channeled cylinder that serves as the cell culture chamber, a membrane holder ring that clamps the membrane, and magnetic ring that allows the device to be secured on the stage of an AFM (A). Before cyclic stretching, VSMCs are allowed to grow on the membrane in an incubator (B). To stretch cells equibiaxially, air is withdrawn from the device to impose a homogeneous strain field throughout the membrane (C).

Calibration of cell extension device

The device was designed to impart an equibiaxial strain distribution in the circular membrane, that is, $\mu_r = \mu_\theta$, where μ_i is a stretch ratio, and subscripts r , θ denote radial and circumferential directions, respectively. In this axisymmetric case, the values of the stretch ratios relative to the x , y directions are same as μ_r , μ_θ (see Appendix), hence the state of strain is equibiaxial independent of coordinate system.

To confirm that the design actually produced a nearly homogeneous (away from the edge effects) and equibiaxial stretch, and to calibrate the degree of stretch in terms of the amount of air infused/withdrawn, we analyzed the response of the membrane in the absence of cells. Briefly, 7 sets of four markers (50-90 μm in diameter, dyed microspheres) were placed on the membrane at several locations and glued with RP30 (Adhesive Systems, Frankfort, IL) (Fig. 3.2A). Three or four adjacent markers in a quadrilateral configuration allow standard interpolation methods for computing the in-plane strains (Humphrey et al., 1987). Images of the tracking markers were captured via a charge-coupled-device (CCD) camera and a video frame-grabber board, which digitizes the image in a 512 x 512 pixel array. For each capture, a search algorithm based on pixel intensity values was used to locate the approximate (± 1 pixel) coordinates for the centroid of each marker. Stretch ratios were then computed by comparing the current marker positions for each set, given by pixel coordinates, relative to the reference positions. Bilinear isoparametric interpolation allowed calculations of the Green strains, and thus stretch ratios, regionally for each set of markers.

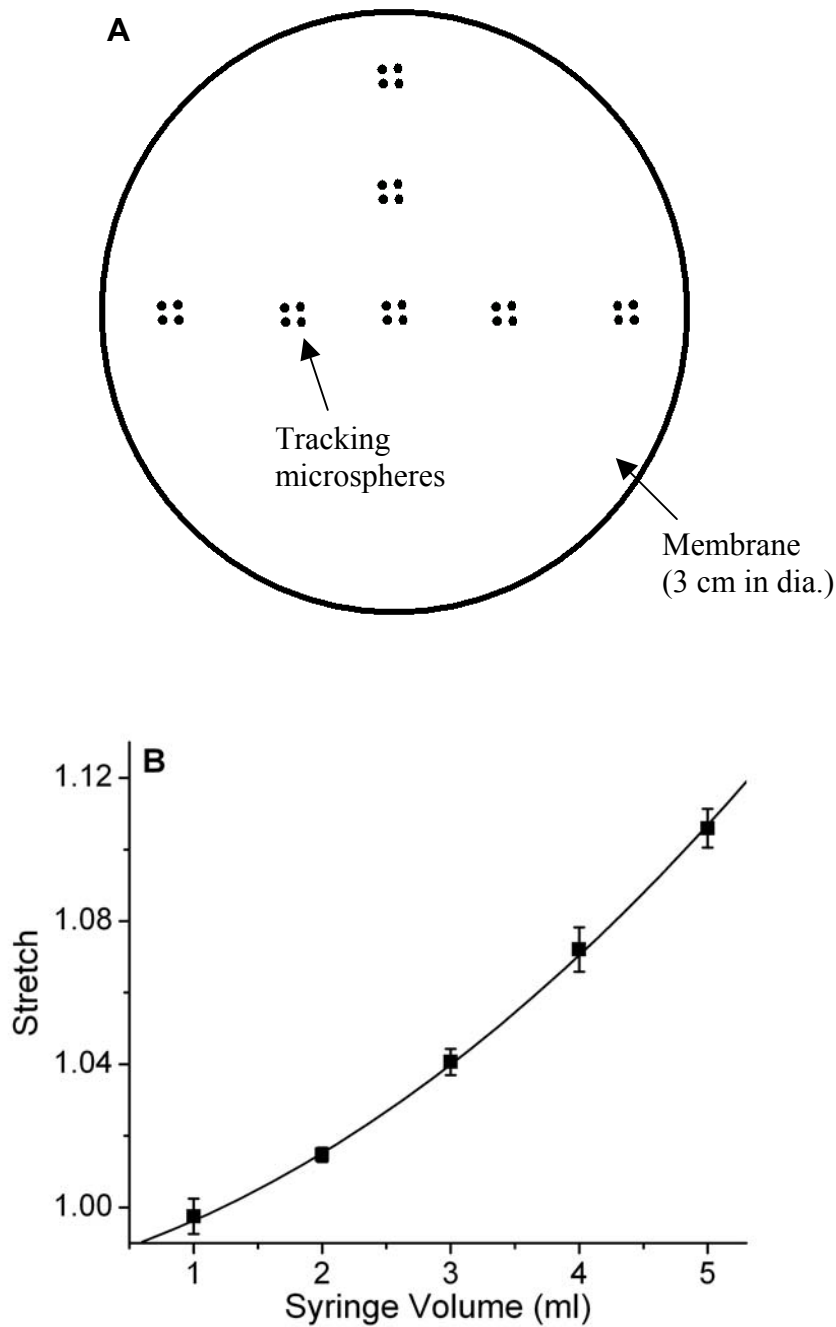


Fig. 3.2. (A) Placement of tracking markers for calibration of membrane stretch as a function of pump volume. Seven sets of four markers are placed on the membrane to confirm homogeneous and equibiaxial stretch. (B) Calibration plot of the mean equibiaxial stretch versus the volume of air infused/withdrawn. Values are means \pm SD. N=24 observations at each point.

Fig. 3.2B shows results for the calibration of stretched membranes. Mean equibiaxial stretch μ is plotted versus the volume V of air infused/withdrawn and was fit with a polynomial relation: $\mu = 0.0029V^2 + 0.0101V + 0.9832$ ($R^2 = 0.9993$). Hence, 5% and 10% stretch required withdrawal of 3.36 ml and 4.84 ml, respectively. Fig. 3.3A shows the near homogeneity of the stretch field, particularly in the central 40% of the membrane, where the standard deviations were small. Fig. 3.3B shows further that the stretch field is indeed nearly equibiaxial, with the dashed line showing the ideal line of identity. Hence, as long as one interrogates cells within the central region, the desired homogeneous, equibiaxial stretches will be attained.

Membrane/device preparation

The membrane and all parts of device were sterilized in 70% ethanol for 30 min, washed 3 times with sterile Dulbecco's phosphate buffered saline (DPBS), and exposed to ultraviolet light for 30 min in a laminar flow hood (Costa et al., 2002). The membrane was then mounted in the device using sterile techniques, and coated with a gelatin for 4 hr at 37°C in a humidified 5% carbon dioxide atmosphere and then washed 3 times with sterile DPBS.

Cell isolation and culture

Vascular Smooth Muscle Cells (VSMCs) were isolated from first order feeder arterioles of rat cremaster muscle using previously described methods (Wu et al., 1998b). Cells were cultured in Dulbecco's modified Eagle's medium (DMEM/F-12) su-

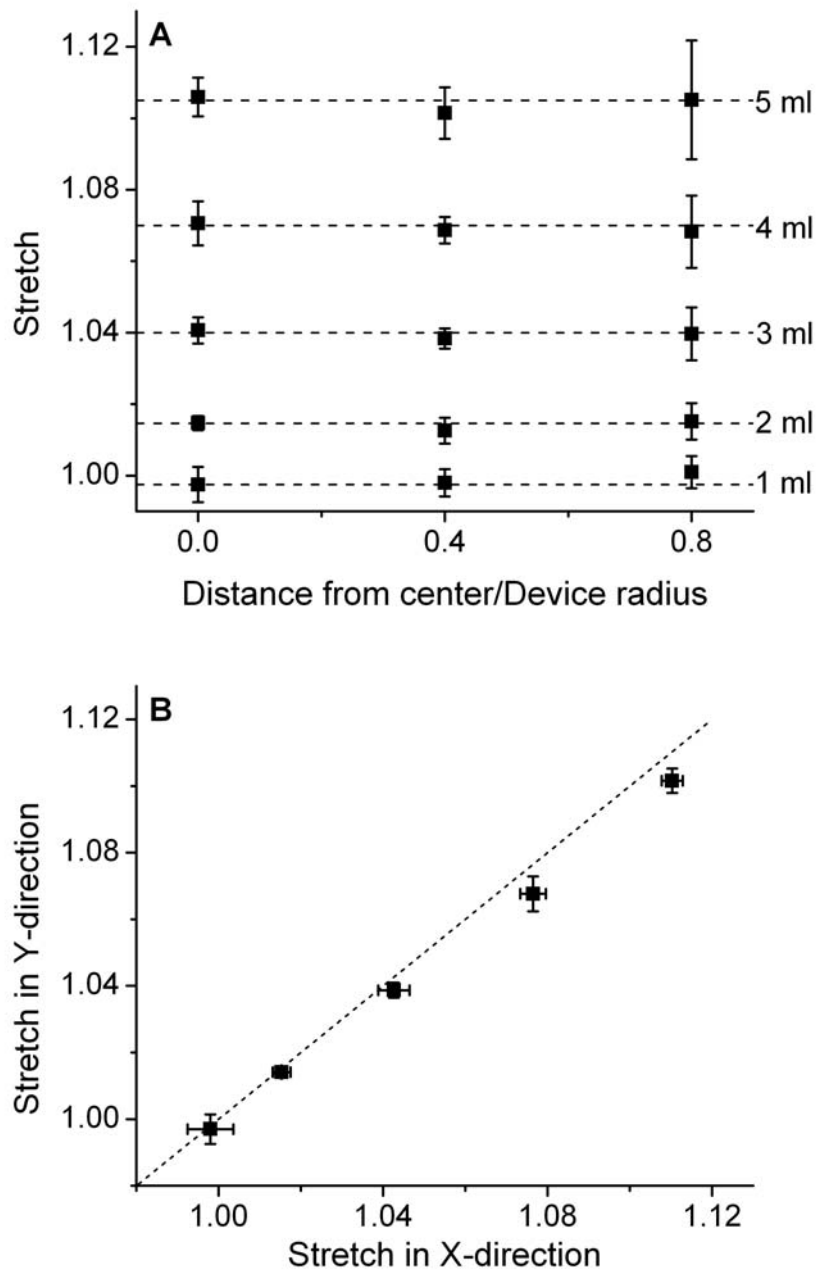


Fig. 3.3. (A) Stretch ratios at various positions along the radius of the membrane. The stretch field is nearly homogeneous, particularly in the central 40% of the membrane, the mean value of which is shown by horizontal dashed line. (B) Stretch ratios in two orthogonal directions (X and Y) in the center during air withdrawal from 1 to 5 ml. Symbols are close to the dashed line of identity, suggesting that stretch field is nearly equibiaxial. Values are mean \pm SD. N=16 observations at each point.

plemented with 10% fetal bovine serum (FBS), and placed in an incubator at 37°C and in humidified 5% carbon dioxide. VSMCs of passages 3-10 were seeded onto the gelatin-coated membrane substrate mounted within the device and were allowed to adhere and spread for 2 to 3 days to reach ~50% confluence.

Stiffness measurements with AFM

Silicon-nitride cantilevers with three types of non-functionalized tips (a pyramidal shape with opening angle of 70°, a 2 μm diameter spherical bead, and a 5 μm diameter bead) were used to examine the effect of tip geometry, and thus the contact area between the tip and the cell. The cantilevers with a pyramidal shape tip (Microlever, Thermomicroscopes, Sunnyvale, CA) had spring constants ranging from 11 to 16 pN/nm. The cantilevers were calibrated using the thermal noise method by Asylum Research Inc. (Santa Barbara, CA), which is subject to an estimated 20% error. Following calibration, we used a mean value of the spring constant of 14.7 pN/nm to estimate cell stiffness. The spring constant of cantilevers with a 2 μm or a 5 μm bead fused to the tip was supplied by the manufacturer (Novascan, Ames, Iowa) as 10 pN/nm. A Bioscope System AFM (Model 3A, Digital Instruments, Santa Barbara, CA) mounted on an Axiovert 100 TV inverted microscope (Carl Zeiss, Thornwood, NY) was used to identify cells and then measure the transverse stiffness. AFM probes were allowed to repeatedly indent and retract from the surface of individual VSMCs in a Force Mode Operation at 0.5 Hz. Tip velocity was 0.8 $\mu\text{m/s}$, which is slow enough to minimize viscous contributions (Mathur et al. 2001). Each cell was indented approximately

halfway between the nucleus and its periphery for 30 s to obtain 15 indentation curves per cell per state of equibiaxial stretch. Five to twelve cells were selected per condition, which is defined by each combination of 0.25 Hz cyclic stretch of $\mu=1.05$ or 1.1, and durations of cyclic stretching of 0, 1, 2, 5, 15, 30, 60 min in each experiment; indentation was performed at a fixed stretch of 1.05 or 1.1 immediately following the cyclic stretching stimulus. Hence, a total of 15 to 25 cells were studied during 2 to 5 independent experiments for each mechanically stimulated condition.

During AFM indentation, the AFM tip exerts a force on the cell that is the product of the spring constant and the deflection of the cantilever. To obtain the cantilever deflection, the initial point of contact between the tip and the cell surface was determined by comparing the slopes of associated force-indentation curves. Indentation depth δ is obtained by subtracting cantilever deflection from piezo movement. Once the force and the tip geometry are known, the stiffness of the cell can be estimated by (Costa and Yin., 1999)

$$\hat{E} = \frac{P}{2\pi f(\delta)}, \quad (3.1)$$

where P is the indentation force obtained from the AFM, and $f(\delta)$ is a function that depends on the tip geometry and the indentation depth. Beatty and Usmani (1975) list the following results for different tip geometries. For a spherical tip of radius a :

$$f(\delta) = \frac{4}{3\pi} \sqrt{a\delta^3}, \quad (3.2)$$

whereas for a conical tip with tip angle 2Φ :

$$f(\delta) = \frac{2 \tan \Phi}{\pi^2} \delta^2. \quad (3.3)$$

Immunofluorescence staining and quantitative analysis of focal adhesions

Dual-labeling immunofluorescence was performed to simultaneously observe the time course of changes in the distribution of F-actin and FA containing vinculin or paxillin. After cyclic stretching, cells were immediately fixed with a 2% paraformaldehyde and quenched with a glycine buffer (0.1 mM glycine). After washing, the cells were incubated overnight at 4°C with either a mouse anti-vinculin or a mouse anti-paxillin monoclonal antibody (Chemicon, Temecula, CA) in labeling buffer (150 mM NaCl, 15 mM $\text{Na}_3\text{C}_6\text{H}_5\text{O}_7$, 0.05% Triton X-100, 2% BSA). Cells were then washed 6 times with a cold washing buffer (150 mM NaCl, 15 mM $\text{Na}_3\text{C}_6\text{H}_5\text{O}_7$, 0.05% Triton X-100), and an Alexa 594-conjugated anti-mouse IgG secondary antibody (Molecular Probes, Eugene, OR) and an Alexa 488-conjugated phalloidin (Molecular Probes) were added for 1 h at room temperature in a dark environment. The fluorescently-labeled cells were washed again with the cold washing buffer, then visualized on a Leica laser confocal microscope system using either a 63x oil or a 63x water immersion objective.

Quantitative analysis of FA proteins was performed on 6 to 7 cells each for two independent experiments per mechanical stretching condition. ImageJ software (NIH, Bethesda, MD) was used to quantify FA areas in terms of an area ratio. This ratio was calculated as the projected total FA area divided by cell area based on immunofluorescence staining of F-actin, vinculin, and paxillin.

Statistical analysis

For analysis of cell stiffness obtained by AFM and area ratios obtained from immunofluorescence images, computed values were expressed as mean \pm SEM unless otherwise noted. Statistical significance compared before and after stretching was calculated by one-way analysis of variance (ANOVA) followed by Dunnett's test (SPSS, Chicago, IL), with $P < 0.05$ considered as significant.

Results

Repeated stiffness measurements (i.e., \hat{E} , in kPa) before and after a single step increase in stretch revealed that cell stiffness did not change significantly during AFM indentation measurement for the ~ 30 min period needed to perform repeated AFM indentations on multiple cells. Shown are results from a single cell tested with a pyramidal shape tip (Fig. 3.4). Panel A shows results over 30 min of repeated indentations in an unstretched (reference) configuration whereas panel B shows results over 30 minutes of testing following a single 15% step increase in equibiaxial stretch. Note that the measurements following stretch also followed an initial ~ 30 min equilibration period. Hence, in response to a 15% stretch, cell stiffness presumably did not change until ~ 50 min after the step increase in stretch. Therefore, from these observations, all stiffness measurements were taken in less than 30 min following stretching in this study.

Force-indentation curves using the aforementioned three different tips revealed an effect of tip geometry on estimated cell stiffness (Fig. 3.5). In each case, stiffness

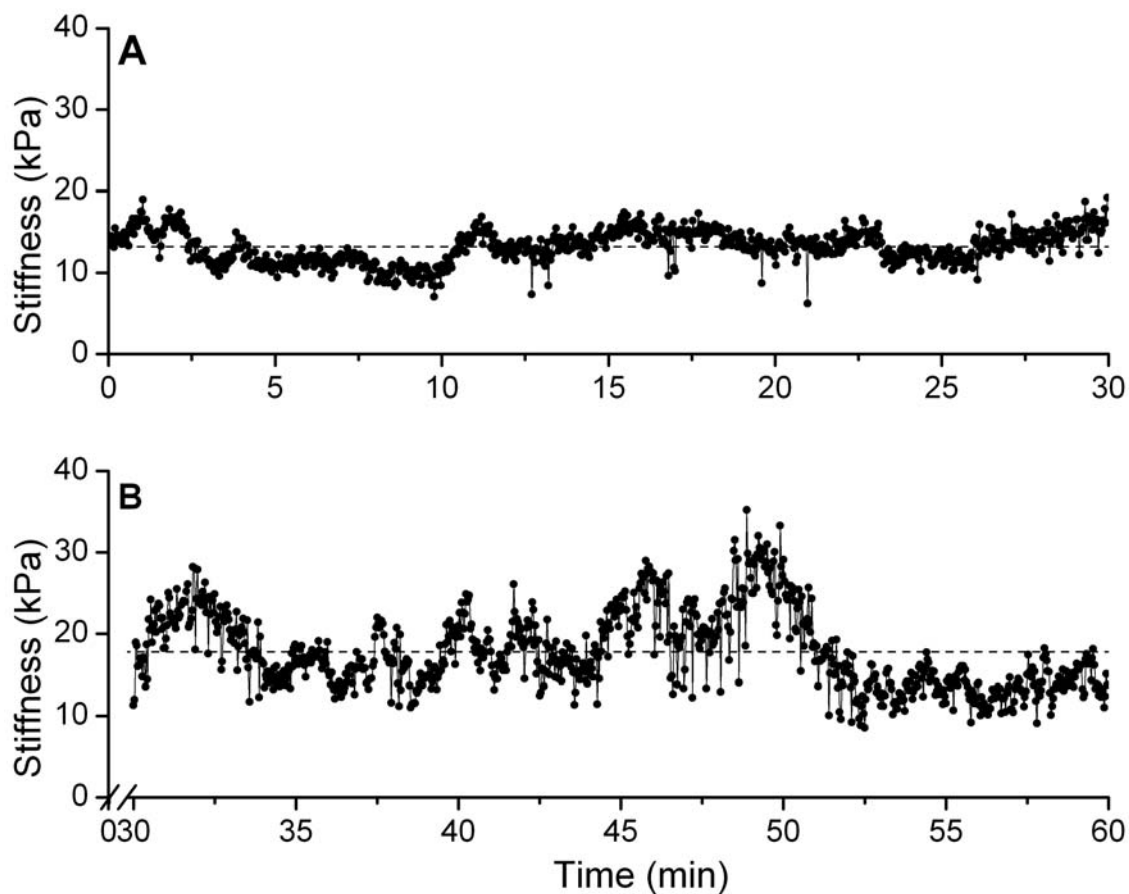


Fig. 3.4. Time course of changes in cell stiffness during AFM indentation measurement. Pyramidal shaped AFM probes repeatedly indented a location halfway between the nucleus and the periphery in a force mode operation at 0.5 Hz (indent for 1 s and retract for 1 s). (A) Stiffness over 30 min of repeated indentations in an unstretched cell. Mean stiffness during indentation, shown as a dashed line, is 13.2 kPa. (B) Stiffness of repeated indentations in response to a single step 15% increase in stretch. The measurements were taken from 30 min to 60 min. Hence, cell stiffness did not change significantly until ~50 min following stretch. Mean stiffness during indentation, shown as dashed line, is 17.8 kPa.

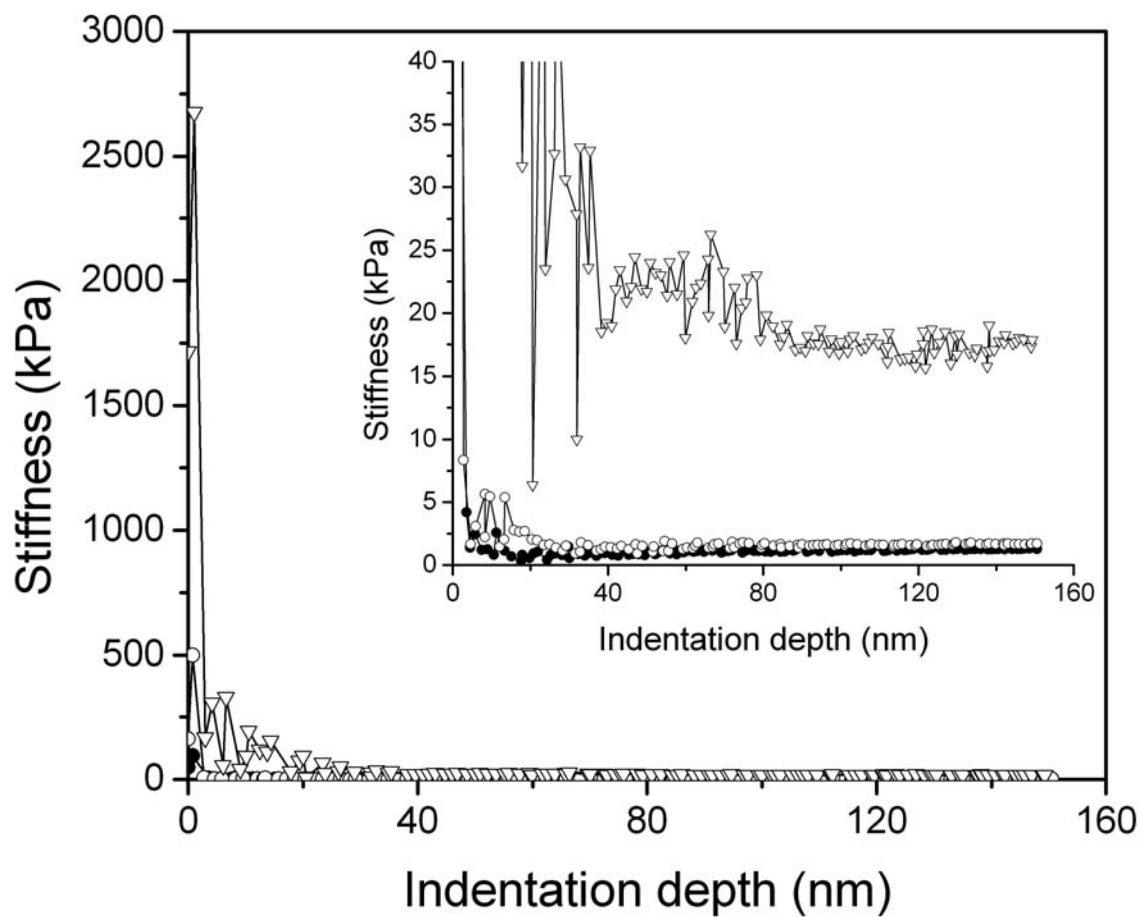


Fig. 3.5. Effect of tip geometry on cell stiffness. ∇ : pyramidal shaped tip; \circ : 2 μm diameter bead tip; \bullet : 5 μm diameter bead tip. Inset is a detail of the low stiffness region of the curves. Note that tip geometry can affect the magnitude of cell stiffness, with a sharp tip yielding both a higher value and variability in cell stiffness.

approached a constant value beyond a certain indentation depth, suggesting no contribution from the substrate for indentation depths in this study (150 nm or less relative to the cell thickness of $\sim 2 \mu\text{m}$). Note, however, that the mean stiffness value obtained from pyramidal shaped tip was $\sim 15 \text{ kPa}$ (Fig. 3.5, inset), which was ~ 10 times that for 2 or 5 μm diameter bead-attached tips. That is, as it is well known, the magnitude of stiffness obtained from AFM can depend on tip geometry. Since the cytoskeleton that plays a critical role in cell stiffness is a highly dynamic structure, indentation with a sharp tip whose characteristic length is similar to the length scale of the cytoskeletal network can yield a high variability in stiffness depending on which region of the cell surface the AFM tip indents, such as on the cytoskeletal filaments or on the fluid-like cytosol. Indentation measurements using tips fused with beads whose dimension is 500~1000 times larger than the diameter of the cytoskeletal filaments produced stable and less noisy results that are more consistent with the underlying continuum assumptions used to estimate the stiffness. Hence, all subsequent results are for indentations with the 5 μm diameter beads.

Fig. 3.6 shows stiffness values for 19 to 24 cells subjected to 10% cyclic stretch for up to 60 min and then held at 10% stretch for ~ 30 min during AFM testing. Note, too, that each bar in the figures shows the mean \pm SD from fifteen stiffness calculations for each cell. Moreover, a different pattern within each bar represents an independent experiment. In the unstretched state, the stiffness values were fairly stable, yielding an average value of 1.30 kPa (N=23 cells from 4 independent experiments), with no trends with time (cf. Fig. 3.4). However, there was a larger variability in stiffen-

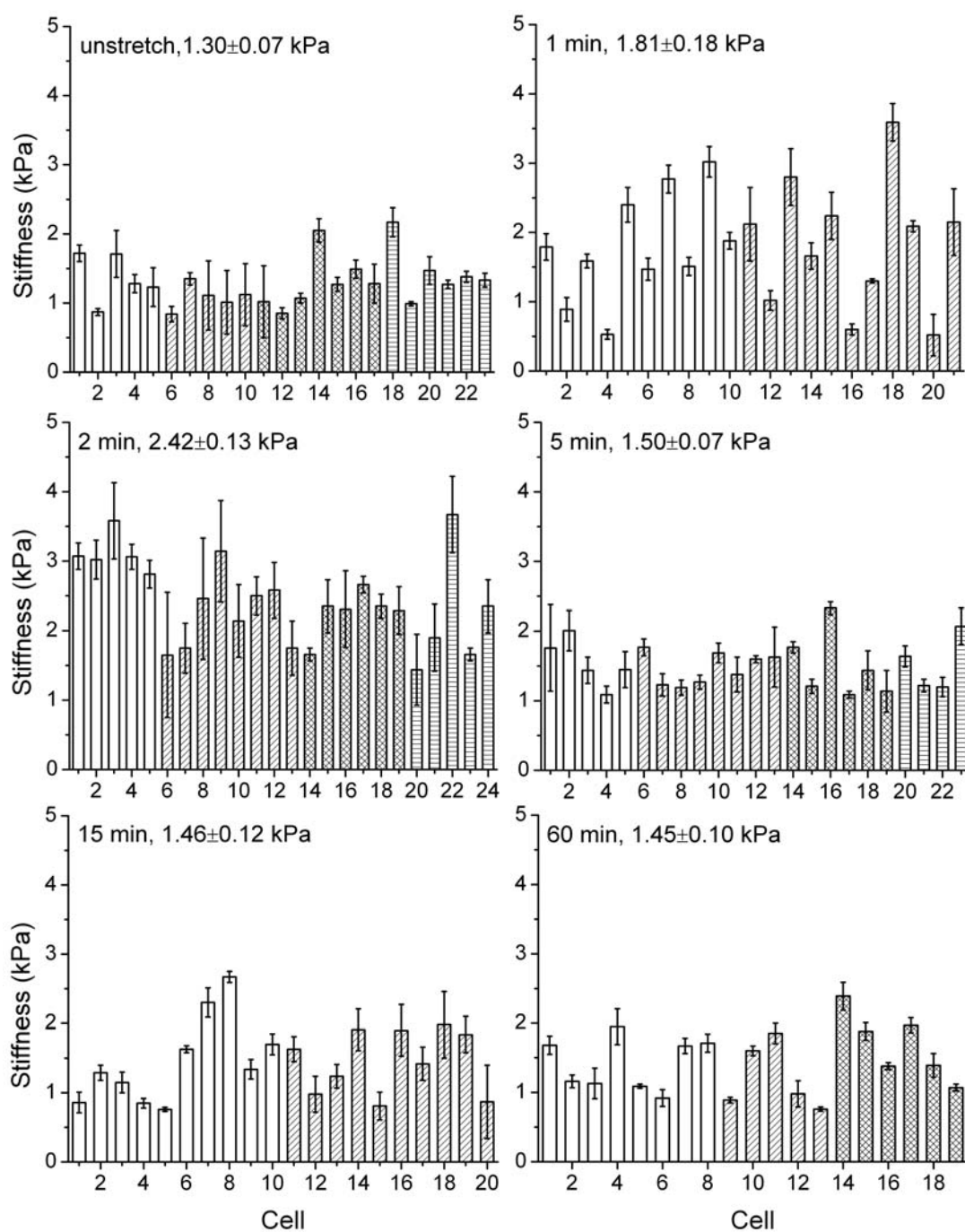


Fig. 3.6. Each bar shows stiffness (mean \pm SD) of individual cells subjected to 10% cyclic stretching. Stretching time and stiffness values (mean \pm SEM) that were combined and averaged per condition are listed in each figure. Different pattern within each bar represents an independent experiment.

-ess 1 min following cyclic stretching. Note that the stiffness values of some cells subjected to cyclic stretching for 1 min were even lower than those of unstretched cells. Stiffness increased significantly and became less variable after 2 min of cyclic stretching, with the mean equal to 2.42 kPa (N=24). Finally, after 5 to 60 min of cyclic stretching, the stiffness decreased back towards a constant value (1.45 kPa), which was 12% higher than baseline.

Fig. 3.7 summarizes the effect of cyclic stretching time (1 to 60 min) and magnitude (5 or 10%) on cell stiffness. Results from 2 to 5 independent experiments per condition were combined and averaged. A 5% cyclic stretching, as a whole, yielded no significant change in stiffness despite a slight increase after 1 and 2 min of stretching with a return towards baseline thereafter. In contrast, a 10% cyclic stretching induced a significant increase in stiffness that was highest after 2 min and returned thereafter towards baseline after 5 min of stretching as seen in Fig. 3.6.

Recent studies showed that increased mechanical loading could recruit FA associated proteins, such as vinculin and paxillin (Sawada and Sheetz, 2002), and increase the thickness of FA (Yoshigi et al., 2005). That is, an increase in FA sites at the basal surface of the cell could reinforce F-actin thus resulting in an increase in stiffness. Based on results in Fig. 3.7, additional cultured cells were subjected to 0.25 Hz, 10% cyclic stretching for 2 min (maximum change in stiffness) or 30 min (stabilized restoration towards baseline), then fixed and stained to examine possible cyclic stretching-dependent cytoskeletal remodeling. A significant increase in vinculin-containing FA area was observed 2 min following cyclic stretch (Fig. 3.8B), which

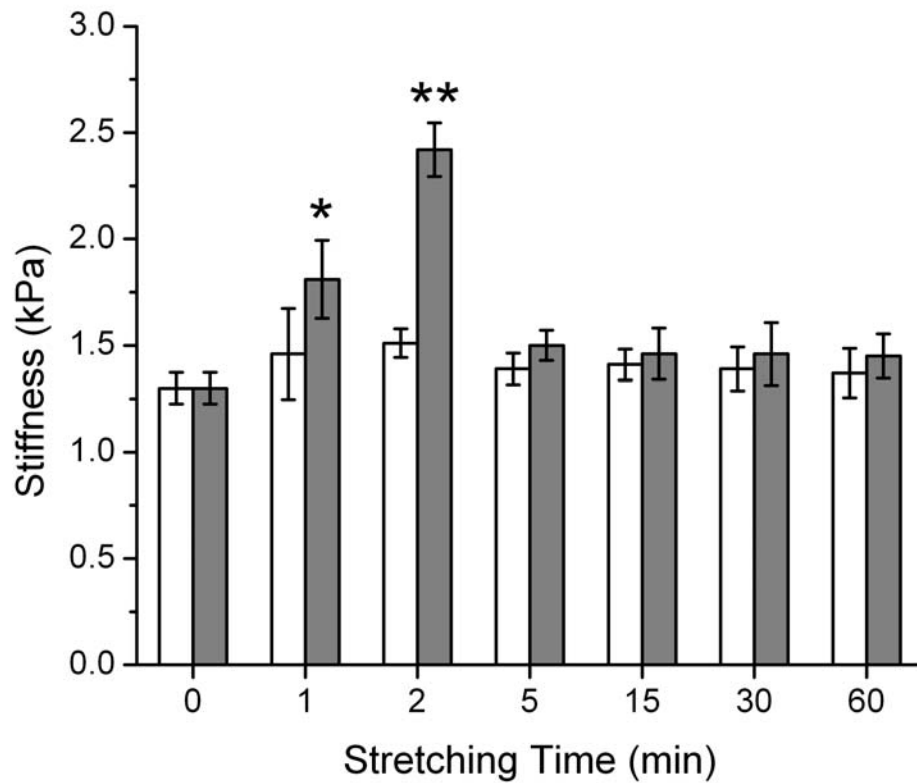


Fig. 3.7. Effect of cyclic stretching time and magnitude on cell stiffness. Mean stiffness values of individual cells per condition are combined and averaged. White and shaded bars represent 5% and 10% stretching, respectively. Results are mean \pm SEM. * shows $P<0.05$ and ** shows $P<0.0001$ compared to the unstretched state. $N=19$ to 24 cells over 2 to 5 independent experiments were performed for each condition.

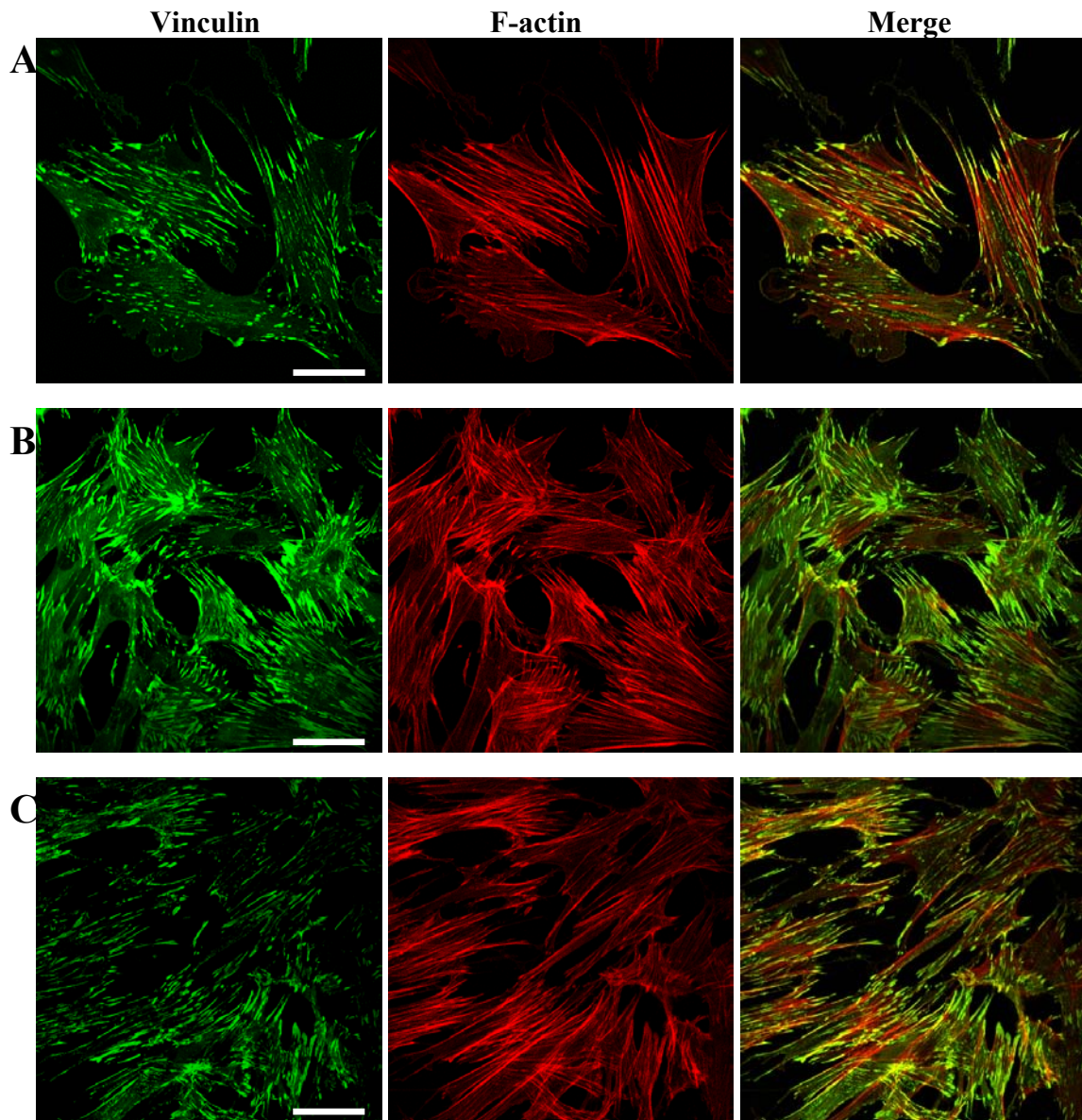


Fig. 3.8. Immunofluorescence micrographs of rat vascular smooth muscle cells. (A) Cells on unstretched membrane. (B) Cells subjected to equibiaxial cyclic stretch (10%, 0.25 Hz) for 2 min. (C) Cells subjected to equibiaxial cyclic stretch (10%, 0.25 Hz) for 30 min. Compared to panels A and C, cyclic stretch for 2 min in panel B induced significant increases in FA associated vinculin staining, particularly at the periphery of the cells. Bars, 50 μ m.

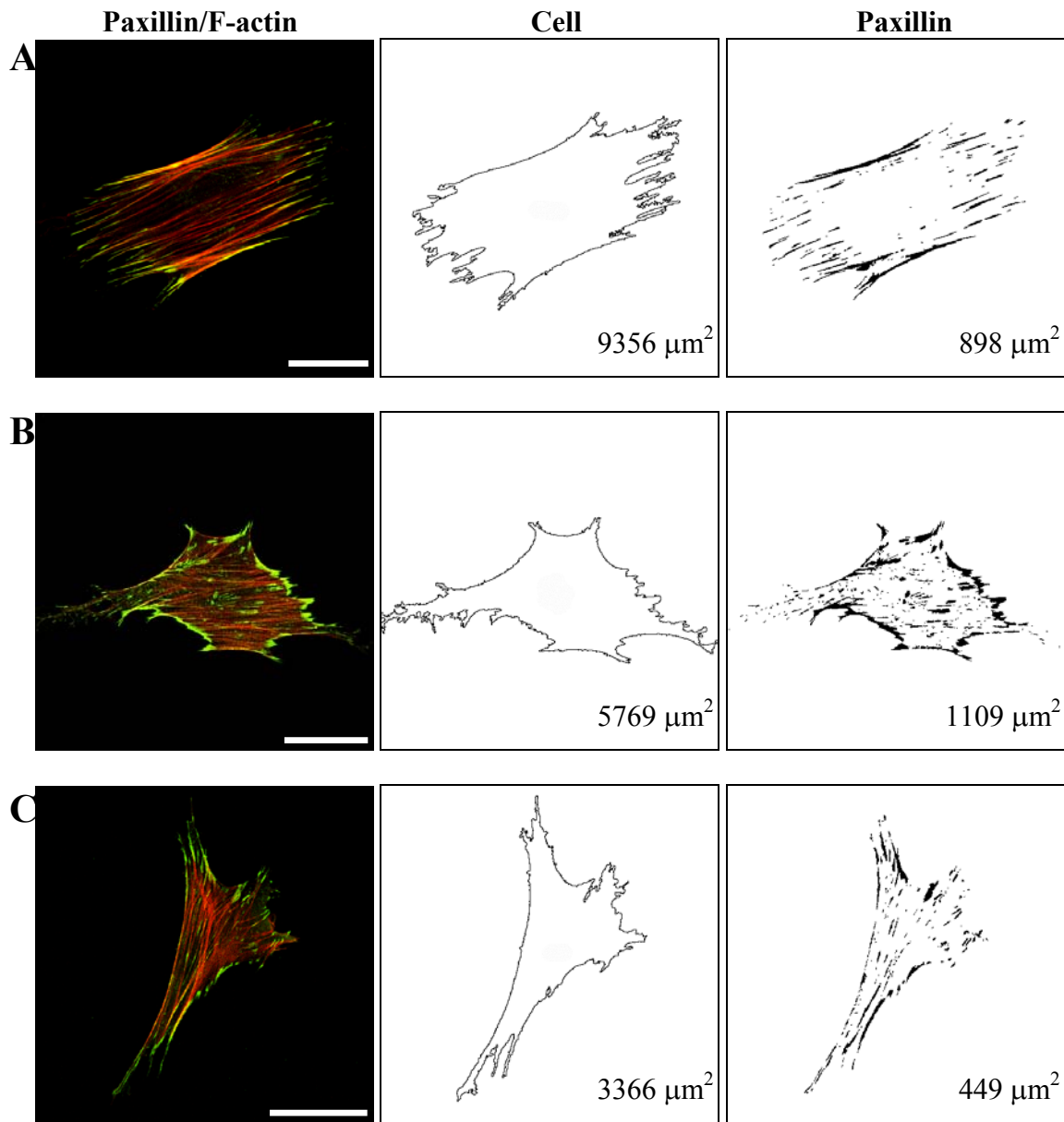


Fig. 3.9. Effect of equibiaxial stretch on focal contact localization. (A) Cells on unstretched membrane. (B) Cells subjected to equibiaxial cyclic stretch (10%, 0.25 Hz) for 2 min. (C) Cells subjected to equibiaxial cyclic stretch (10%, 0.25 Hz) for 30 min. Note that cyclic stretch for 2 min in panel B induced significant increases in FA associated paxillin staining, particularly at the periphery of the cells. Projected cell area and the paxillin-containing FA area were also quantified in the middle and right column, respectively. Bars, 50 μm .

was consistent with changes in stiffness inferred with the AFM. Vinculin area returned towards the unstretched level albeit slightly higher following 30 min of cyclic stretching (Fig. 3.8C). Changes in the area of FA associated paxillin in response to cyclic stretching were consistent with those of vinculin (Fig. 3.9), with a stretch-dependent accumulation of paxillin observed at FA sites.

Finally, to study relationships between cell stiffness and cytoskeletal remodeling in response to cyclic stretching, projected cell area and FA area based on immunofluorescence dual labeling of vinculin/paxillin were compared (Fig. 3.10). FA area was divided by the corresponding cell area to generate an area ratio, which represents the fraction of FA at the basal surface of a cell. Area ratio corresponding to vinculin was found to increase by 49% after 2 min of cyclic stretching, but to return towards baseline after 30 min of stretching. FA associated paxillin increased in a similar manner, but with a much larger magnitude (92%) than noted for vinculin (Fig. 3.10). In summary, there was a close relationship between stretch induced increase in cell stiffness and area ratio corresponding to FA associated vinculin and paxillin (Fig. 3.11).

Discussion

Observations from diverse studies on cell biomechanics and mechanobiology reveal that altered mechanical stretching can induce changes in CSK structure and overall mechanical properties. The objective of this study was to investigate relationships between cell stiffness and FA remodeling in response to cyclic stretching.

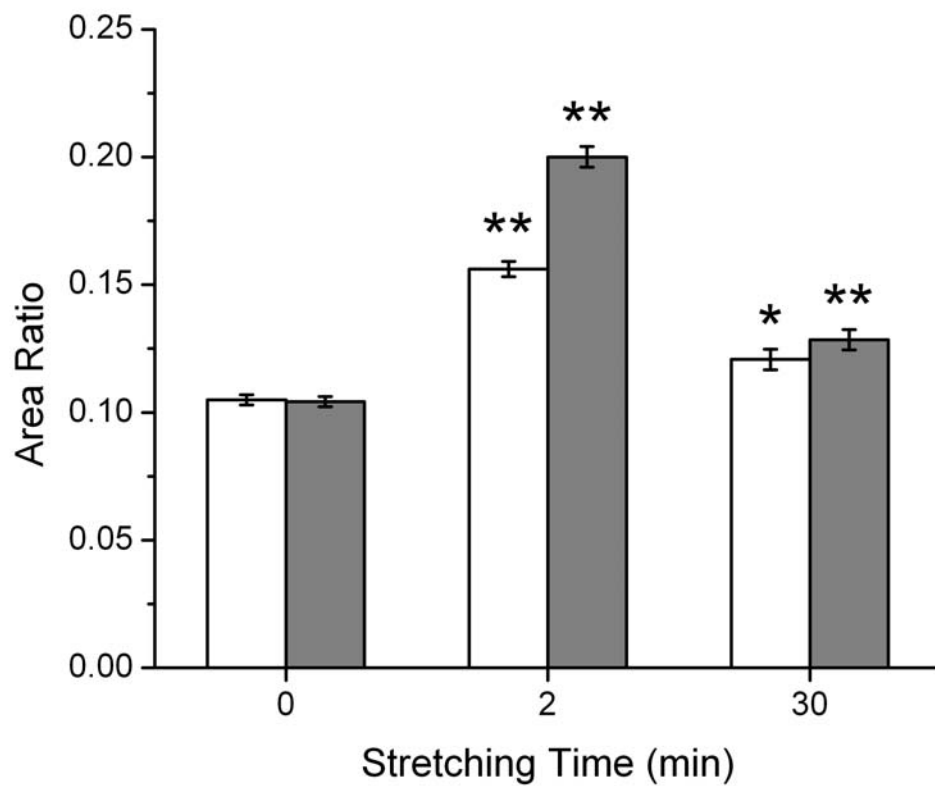


Fig. 3.10. Ratio of FA associated vinculin (open) and paxillin (shaded) area to corresponding projected cell area in response to stretching time. Cells were subjected to 0.25 Hz, 10% cyclic stretching for 2 or 30 min. Results are mean \pm SEM. * shows $P < 0.005$ and ** shows $P < 0.0001$ compared to the corresponding unstretched state. Experiments for vinculin and paxillin were performed independently. N=6 to 7 cells each for two independent experiments per condition.

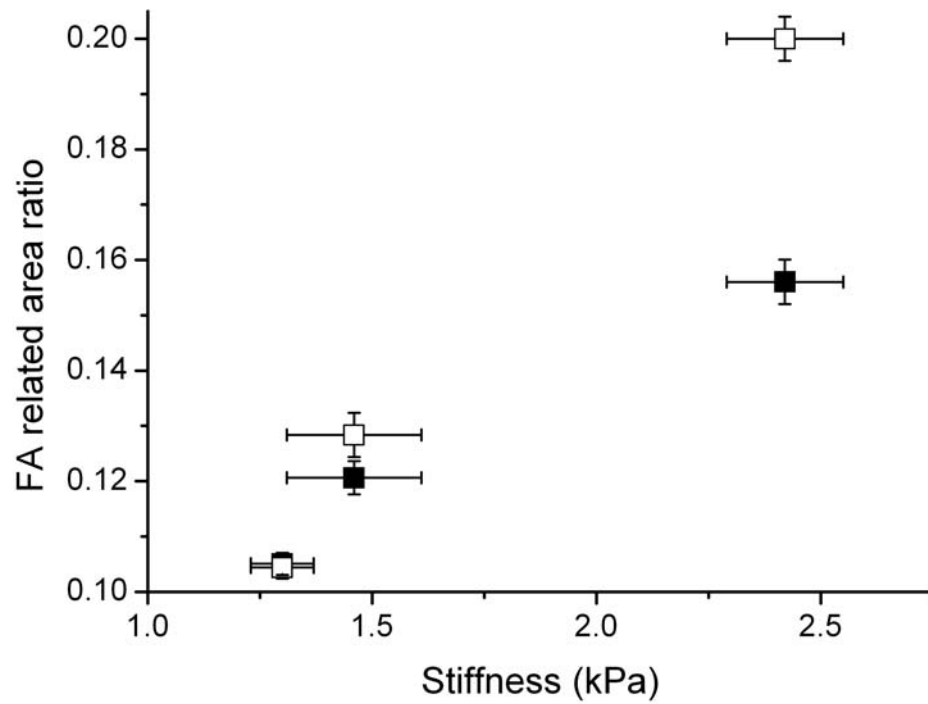


Fig. 3.11. Correlation between cell stiffness and FA associated vinculin/paxillin area ratio in response to 10% cyclic stretch. ■: vinculin; □: paxillin. Results are mean \pm SEM.

Toward this end, AFM combined with a cell extension device allowed real-time measurement of cell stiffness following cyclic stretching. To employ a continuum-based approach for quantifying cell stiffness (Costa and Yin, 1999), we used AFM tips fused with 2 μ m or 5 μ m diameter beads whose dimension is 500~1000 times larger than the diameter of the CSK filaments. This selection is supported by the findings of Mathur et al. (2001), who compared the effect of tip geometry on cell stiffness. They found that blunt cone-spherical tips produced more stable and lower stiffness values compared to sharp conical tips, which is consistent with our study. That is, indentation with a sharp tip whose characteristic length is similar to the diameters of the CSK filaments can yield a high variability in stiffness depending on which region of the cell surface the AFM tip indents, which is not consistent with the underlying continuum assumptions used to estimate cell stiffness. For example, Mizutani et al. (2004) used pyramidal tips and reported large variabilities in stiffness, from 0.7 to 40 kPa. In contrast, 5 μ m diameter beads used herein produced a fairly stable range of stiffness values (see Fig. 3.6) except for 1 min cyclic stretching, which is discussed below. Although the magnitude of cell stiffness measured in this study using 5 μ m diameter tips (1~3 kPa) was lower than that of previous studies using sharp pyramidal or conical tips, it was very similar to the range (0.1~10 kPa) obtained from most other techniques for mechanically probing cells, including optical traps, magnetic traps, or magnetic twisting (Huang et al., 2004).

Previous studies have shown that altered mechanical stimuli can alter cell stiffness under very different conditions. Smith et al. (2003) found changes in cell stiffness after 10~12 days of continuous cyclic stretching, a very different time frame

from that of our study. Deng et al. (2004) reported the time course of changes in cell stiffness in response to twisting integrin-bound microbeads, which is a much more localized stimulus than that due to substrate stretch. Mizutani et al. (2004) found increases (decreases) in stiffness following a single step increase (decrease) in substrate stretch, which were followed by gradual (over 50 min) returns towards baseline values. They used AFM with a force-mapping mode that provides height and stiffness images of a sample by scanning a cell on certain area, which requires ~30 min to get mean stiffness value at one spot. Hence, this approach is not appropriate to capture rapid and detailed changes of cell stiffness within even a minute.

Our study showed that cyclic stretching induced rapid increases in cell stiffness (within 1 min, but marked at 2 min) that were soon resolved (within 5 min) in that stiffness returned back towards normal and remained as such over long periods (up to 50 min). Such rapid responses are consistent with studies by Costa et al. (2002) and Cunningham et al. (2002). That the measured stiffness was particularly variable after 1 min of cyclic stretching (Fig. 3.6) may reflect a transient period with slight differences between the timing within individual cells. Pender and McCulloch (1991) showed, using fluorimetry, that F-actin decreased up to 3-fold within only 10 s of 1% stretch and back towards baseline after 75 s. It is easy to imagine, therefore, that 1 min of 10% cyclic stretching could be within a transition period during which rapid turnover of F-actin occurs: cells undergo F-actin disruption with reassembly ~1 min following cyclic stretching. We note, too, that both mechanical stimuli and contractile stimulation can change cell stiffness that is brought about by CSK remodeling (Deng et al., 2004; Saez et

al., 2004). Interestingly, the degree of stiffness increase as well as corresponding time frame in our study is quantitatively consistent with the time course of the response of smooth muscle cells to KCl, a contractile agonist (Smith et al., 2003), although little is known about the relation between mechanical and chemical stimuli.

Consistent with the biochemical data from Cunningham et al. (2002), cyclic stretching induced rapid changes in FA localization (Figs. 8 and 9). Cells subjected to 10% cyclic stretching for 2 min exhibited a significant increase in FA area compared to unstretched cells. Because fluorescence intensity of FA was very strong at the basal surface, whereas that of F-actin is highly dependent on the focal plane within variable thickness of cells, we chose to quantify FA area. Quantitatively consistent with Cunningham et al. (2002), FA associated vinculin area ratio increased by ~50% and FA associated paxillin area ratio by ~90% at 2 min and then returned towards baseline by 30 min.

In summary, this study demonstrates that cyclically stretching isolated VSMCs significantly and rapidly alters both cell stiffness and FA associated vinculin and paxillin. That cell stiffness correlated well with FA remodeling suggested that FA remodeling could play a critical role in cell stiffness by recruiting and anchoring F-actin. It is not clear, however, whether this rapid change in cell stiffness following cyclic stretching is due to F-actin polymerization or the development of additional tensile force in F-actin generated by the phosphorylation of paxillin. Additional studies on the biochemical consequences of cyclic stretching will provide further insight into how cells sense and respond to their mechanical environment.

CHAPTER IV
TIME-DEPENDENT CHANGES IN CYTOSKELETAL REMODELING
IN RESPONSE TO CYCLIC STRETCH: A THEORETICAL STUDY
BASED ON EXPERIMENTAL DATA

Introduction

The cytoskeleton (CSK) not only provides a structural framework that determines cell shape and mechanical properties, it also influences many important cellular functions (Bray, 2000; Alberts et al., 2002). Within a tissue environment, a variety of extracellular stimuli, including fluid-induced shear or matrix-induced stretch, affect the distribution and organization of the CSK filaments (e.g., Smith et al., 1997; Galbraith et al., 1998; Takemasa et al., 1998; Wang et al., 2000, 2001; Hayakawa et al., 2001; Costa et al., 2002; Yoshigi et al., 2003). Accordingly, many different types of mathematical models have been derived to predict mechanosensitive responses of living cells (for a review, see Zhu et al., 2000; Stamenovic and Ingber, 2002; Bao and Suresh 2003; Huang et al., 2004; Lim et al., 2006). All of these models of cell mechanics have been based on either standard continuum models (based on the assumptions of material uniformity) or microstructural models based on assumed orientations, distributions, and material behaviors of individual CSK filaments (e.g., tensegrity). Recently, Humphrey (2002a) proposed a fundamentally different approach based on the concept of a constrained mixture, which is a microstructurally motivated continuum model that allows individual constituents to turnover dynamically. This approach allows one to

include the separate contributions and distributions of the primary CSK filaments and viscous cytosol without having to solve separate balance relations for each constituent, to quantify possible momentum exchanges between constituents, or to prescribe partial traction boundary conditions which are notoriously difficult to identify. Thus, this approach can provide details on locally averaged distributions of stresses and strains in cells, which in turn can be useful in determining the distribution and transmission of forces to subcellular components.

Recent studies show that a single step (static) increase of substrate stretch can induce an immediate increase in cell stiffness (Mizutani et al., 2004) as well as alter the area of focal adhesion (FA) associated vinculin (Sawada and Sheetz, 2002). In our recent experiments (Na et al., 2006), we found that rapid changes in cell stiffness in response to cyclic stretching relate closely to FA recruitment. In this study, therefore, we seek to use a constrained mixture approach to model CSK remodeling by synthesizing data on stretch-induced dynamic changes in cell stiffness and focal adhesion area. Toward this end, the model was fitted to force-indentation curves obtained from atomic force microscopy (AFM) measurements of cyclically stretched vascular smooth muscle cells.

Materials and methods

Details on the cell culture methods, design of the cell stretching device, and data collection from AFM and confocal microscopy experiments are in Na et al. (2006); here we simply provide a brief review as background. Fig. 4.1 is a flow chart showing an overall synthesis of experiments and modeling.

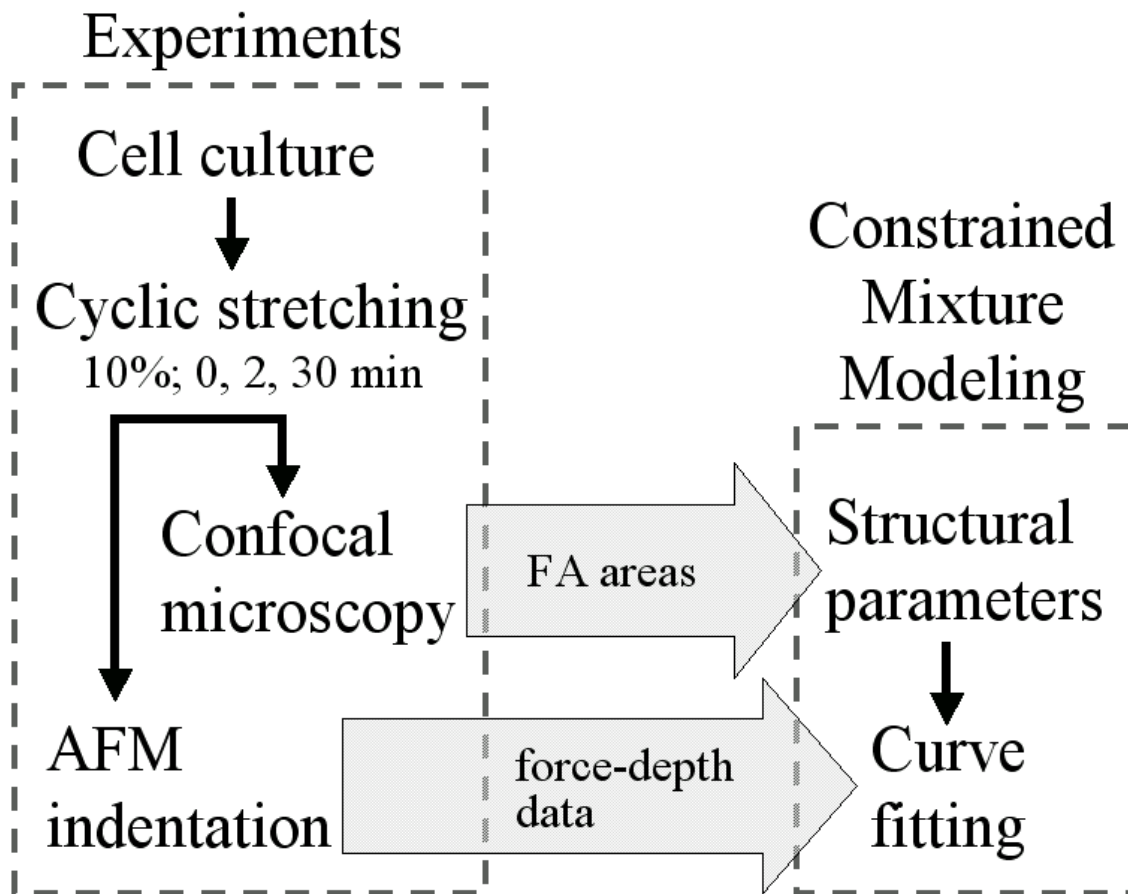


Fig. 4.1. Flow chart showing a synthesis of experiments and modeling. In this study, results from prior experiments on vascular smooth muscle cells were used to predict cytoskeletal (CSK) remodeling in response to cyclic stretching. Values of focal adhesion (FA) associated vinculin area obtained from immunostaining and confocal microscopy were used as parameters in a mixture model of CSK remodeling. The model was then fitted with force-indentation data obtained from AFM measurements to predict time-dependent CSK remodeling in response to cyclic stretching,

Experimental protocol

Briefly, Vascular Smooth Muscle Cells (VSMCs) from first order feed arterioles within rat cremaster muscle were isolated, expanded through 3 to 10 passages, and cultured in Dulbecco's modified Eagle's medium (DMEM/F-12), supplemented with 10% fetal bovine serum, on a custom stretching device that can be secured on the stage of an AFM. The device applies a cyclic, homogeneous, equibiaxial stretch to the central region of a circular silicone elastic membrane by dynamic infusion and withdrawal of air using a programmable syringe pump. VSMCs were cyclically stretched 10% at a frequency of 0.25 Hz with durations of stretching of 2 or 30 min.

A Bioscope System atomic force microscope (AFM; Digital Instruments, Santa Barbara, CA) mounted on an Axiovert 100 TV inverted microscope (Carl Zeiss, Thornwood, NY) was used to obtain force-indentation curves for individual cells. AFM probes consisting of silicon-nitride cantilevers fused with a 5 μ m spherical bead were allowed to repeatedly indent and retract from the surface of VSMCs in a Force Mode Operation at 0.5 Hz. Tip velocity was 0.8 μ m/s, which is slow enough to minimize viscous contributions from the cytosol (Mathur et al. 2001). Each cell was indented halfway between the nucleus and its periphery for 30 s to obtain 15 indentation curves per cell per duration of equibiaxial cyclic stretching. Five to twelve cells were selected per plate, and two to five independent experiments were performed per mechanical stretching condition for a total of 15-25 cells for each condition.

Immunofluorescence staining was performed independently. After cyclic stretching, cells were immediately fixed with a 2% paraformaldehyde and quenched with

a glycine buffer (0.1 mM glycine). After washing, the cells were incubated with a mouse anti-vinculin monoclonal antibody, an Alexa 594-conjugated anti-mouse IgG secondary antibody, and an Alexa 488-conjugated phalloidin. The fluorescently-labeled cells were visualized on a Leica laser confocal microscope system using either a 63x oil or a 63x water immersion objective.

Quantitative analysis of focal adhesion proteins was performed on 6~7 cells each for two independent experiments per mechanical stretching condition (10% cyclic stretching for 2 or 30 min, respectively). FA area ratio was calculated using ImageJ software as the projected total FA area divided by cell area based on immunofluorescence staining of actin filaments (F-actin) and vinculin.

CSK remodeling model

We employed a constrained rule-of-mixtures model for the CSK, which for the case of a single change in stretch (unstretched to 10% stretch) can be written generally as (recall Eq. 2.1.)

$$\begin{aligned} \mathbf{t} = & -p\mathbf{I} + \phi^c 2\tilde{\mu}\mathbf{D} + \phi_o^a \mathbf{t}^a(\mathbf{F}_{\kappa_o^a}) + \phi_o^i \mathbf{t}^i(\mathbf{F}_{\kappa_o^i}) + \phi_o^m \mathbf{t}^m(\mathbf{F}_{\kappa_o^m}) \\ & + \phi_n^a \mathbf{t}^a(\mathbf{F}_{\kappa_n^a}) + \phi_n^i \mathbf{t}^i(\mathbf{F}_{\kappa_n^i}) + \phi_n^m \mathbf{t}^m(\mathbf{F}_{\kappa_n^m}) \end{aligned} \quad (4.1)$$

where p is a Lagrange multiplier that enforces incompressibility over transient loading, \mathbf{D} is the stretching tensor (i.e., $2\mathbf{D} = \dot{\mathbf{F}}\mathbf{F}^{-1} + \mathbf{F}^{-T}\dot{\mathbf{F}}^T$ where the over-dot denotes a time-derivative), $\tilde{\mu}$ is a viscosity associated with the cytosol, the \mathbf{F}_{κ} 's are deformation gradient tensors for each constituent relative to individual natural configurations κ_o

(original) or κ_n (new), and the ϕ 's are mass fractions (i.e., constituent mass per total mass) of individual constituents, which by definition are subject to the constraint

$$\phi^c + \phi_o^a + \phi_o^i + \phi_o^m + \phi_n^a + \phi_n^i + \phi_n^m = 1. \quad (4.2)$$

Whereas the subscript o denotes “original” and n denotes “new,” the superscripts c , a , i , and m denote cytosol, actin, intermediate filaments, and microtubules, respectively. This basic framework allows one to include nonlinear elasticity and viscoelasticity, different properties and distributions of individual constituents, and, most importantly, different rates and extents of turnover of individual constituents.

Although each family of CSK filaments plays a role in maintaining cell shape (Ingber, 1993), F-actin has been shown to impart the primary mechanical stiffness of living cells (Wu et al., 1998a; Rotsch and Radmacher, 2000; Wakatsuki et al., 2000) and to be physically connected to FA sites at the basal membrane (Mitra et al., 2005). Indeed, our previous modeling results also showed that removal of intermediate filaments and microtubules reduced cell stiffness less than 10% (Na et al., 2004). Herein, therefore, we focus exclusively on F-actin. Although cells exhibit viscoelastic character under various types of loading, our AFM experiments used a slow tip velocity compared to the viscoelastic time constants. Therefore, we restrict our attention to the elastic response of F-actin to estimate AFM measured CSK remodeling. In the absence of contributions from intermediate filaments, microtubules, and cytosol, therefore, Eq. 4.1 simplifies to

$$\mathbf{t} \cong -p\mathbf{I} + \phi_o^a \mathbf{t}^a \left(\mathbf{F}_{\kappa_o^a} \right) + \phi_n^a \mathbf{t}^a \left(\mathbf{F}_{\kappa_n^a} \right), \quad (4.3)$$

where o denotes “originally present” and n denotes “newly formed or assembled.” We emphasize that there was not sufficient time to synthesize new F-actin.

Here, therefore, recall the general form for the Cauchy stress that is required by the Clausius-Duhem inequality for an isochoric elastic process:

$$\mathbf{t} = -p\mathbf{I} + 2\mathbf{F}\frac{\partial W}{\partial \mathbf{C}}\mathbf{F}^T, \quad (4.4)$$

where W is a strain energy function and \mathbf{C} is the right Cauchy-Green tensor (i.e., $\mathbf{C} = \mathbf{F}^T\mathbf{F}$ where superscript T denotes transpose). Here, we construct a strain energy function for potentially evolving F-actin. We emphasize that the resulting relations are microstructurally-motivated (Lanir, 1983), but phenomenological. Hence, let

$$W \equiv W^a = \sum_{k=1}^N \phi_k^a \int_0^{2\pi} \int_{-\pi/2}^{\pi/2} R_k^a(\varphi, \theta) w_k^a(\alpha_k) \cos \varphi d\varphi d\theta, \quad (4.5)$$

where $w_k^a(\alpha_k)$ is a 1-D strain energy function for F-actin and α_k is its stretch relative to an individual, evolving natural configuration. The subscript k denotes the constituent family (original or new), which is to say denotes the related natural configuration of the F-actin (e.g., $k=1$ and 2 denotes original and new, respectively). The function $R_k^a(\varphi, \theta)$ represents the original distribution of orientations of F-actin and ϕ_k^a is the associated mass fraction. The superscript a representing F-actin is omitted below without ambiguity. Clearly, Eqs. 4.4 and 4.5 yield the same “model” as Eq. 4.3 provided one accounts for relationships between the overall and individual reference configurations (Baek et al., 2006). For simplicity and because of difficulties of measuring 3-D distributions of filaments, let $R_k(\varphi, \theta) = 1/4\pi$, assuming that all filaments are originally

distributed isotropically (which is likely prior to adhesion and spreading), although they will reorient with deformation. Substituting Eq. (4.5) into Eq. (4.4) gives

$$t_{ij} = -p\delta_{ij} + 2 \sum_{k=1}^N \phi_k \left(\int_0^{2\pi} \int_{-\pi/2}^{\pi/2} R_k(\varphi, \theta) \frac{\partial w_k}{\partial \alpha_k} \frac{1}{2\alpha_k} \frac{\partial C'_{11}}{\partial C_{MN}} \cos \varphi d\varphi d\theta \right) F_{iM} F_{jN}. \quad (4.6)$$

where the 1' (i.e., primed) coordinate axis coincides with the direction of a generic filament, and C'_{11} is obtained from a tensorial transformation of C_{MN} .

Consistent with previous reports that the mechanical behavior of individual CSK filaments is qualitatively similar to those of soft tissue (Janmey et al., 1991; Liu and Pollack 2002; Deguchi et al., 2006), two specific functional forms of the first Piola-Kirchhoff stress-stretch relation ($\partial w / \partial \alpha$) for the individual CSK filaments were compared (Humphrey and Yin, 1987b; Misof et al., 1997):

$$\frac{\partial w}{\partial \alpha} = cc_1(\alpha - 1) \left[\exp\left(c_1(\alpha - 1)^2\right) \right]; \text{ exponential model}, \quad (4.7)$$

$$\frac{\partial w}{\partial \alpha} = \frac{cc_1(\alpha - 1)}{\alpha(c_1 - (\alpha - 1))}; \text{ Misof model}, \quad (4.8)$$

where c and c_1 are separate material parameters for F-actin. Note, here, that we assume that intrinsic material properties of “original” and “new” F-actin are same; only the orientations, mass fractions, and natural configurations evolve. Hence, material parameters, c and c_1 , are assumed to be constant during CSK remodeling.

Application of CSK remodeling model to AFM indentation

Detailed analysis of an AFM indentation superimposed on a finite equibiaxial stretch was described previously (Na et al., 2004). Briefly, the force versus indentation depth (P - δ) relationship is (Beatty and Usmani, 1975; Green et al., 1952):

$$P = 2\pi \frac{\Gamma(W)}{\Sigma(W)} \hat{f}(\delta), \quad (4.9)$$

where $\Gamma(W)$ and $\Sigma(W)$ are functionals that depend on the strain-energy function W and the in-plane finite equibiaxial stretch μ whereas the function $\hat{f}(\delta)$ depends on the geometry of the tip of the rigid indenter. A spherical tip of radius a is used in this study, therefore (Beatty and Usmani, 1975),

$$\hat{f}(\delta) = \frac{4}{3\pi} \sqrt{a\delta^3}. \quad (4.10)$$

To compute $\Gamma(W)$ and $\Sigma(W)$, we need the strain energy function W in terms of invariants I_i of the right Cauchy-Green tensor \mathbf{C} . Since the proposed strain energy function for CSK remodeling is written in terms of stretch α , which is related to \mathbf{C} , we can easily find the requisite relations between derivatives with respect to the invariants I_i and those in terms of the components of \mathbf{C} (Na et al., 2004). These results are used without restatement here.

Results

Fig. 4.2 shows representative immunofluorescence micrographs as well as corresponding projected total cell areas and FA associated vinculin areas in response to

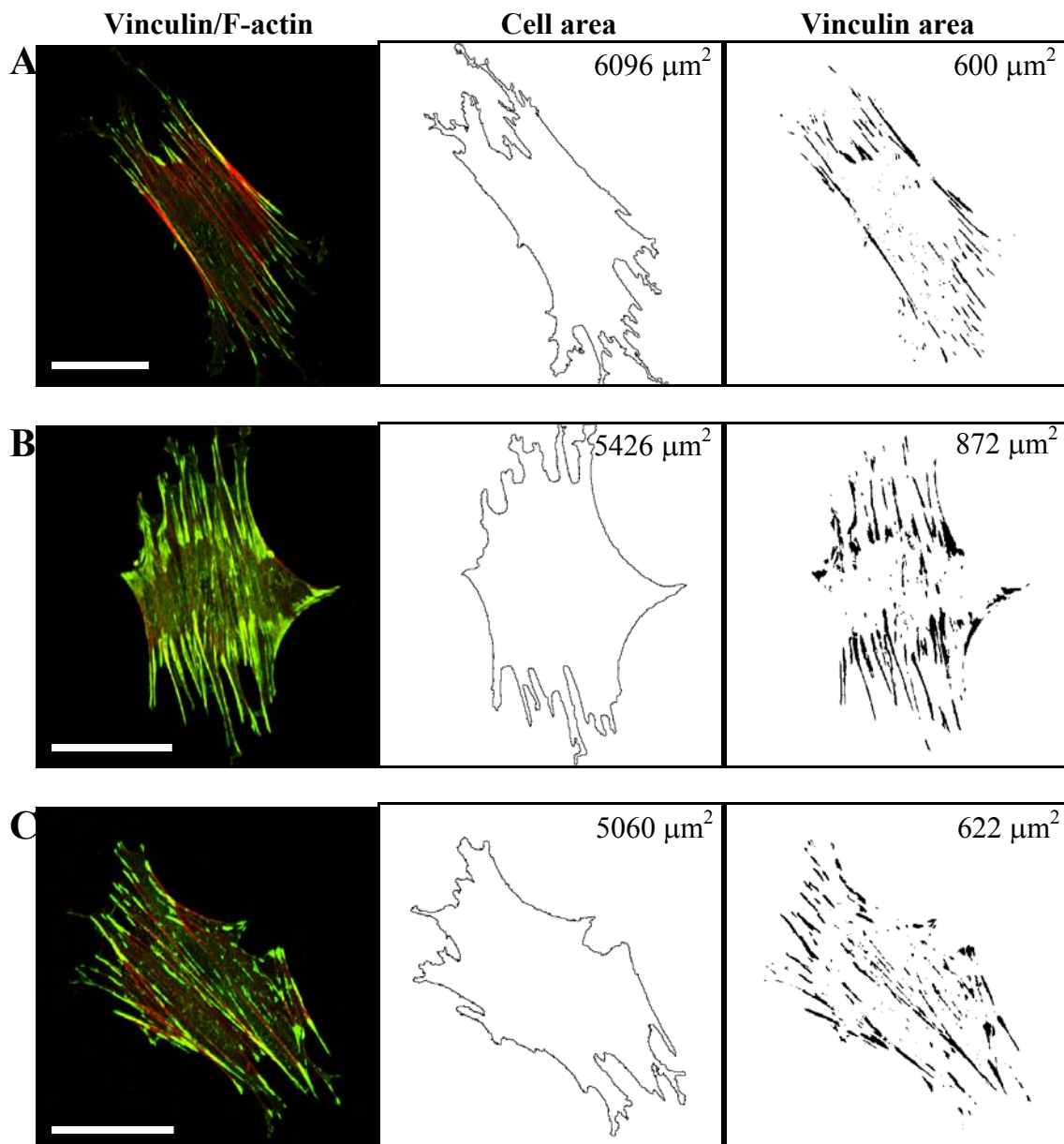


Fig. 4.2. Effects of equibiaxial stretch on FA localization. (A) Cells on unstretched membrane. (B) Cells subjected to equibiaxial cyclic stretch (10%, 0.25 Hz) for 2 min. (C) Cells subjected to equibiaxial cyclic stretch (10%, 0.25 Hz) for 30 min. Note that cyclic stretch for 2 min in panel B induces a significant increase in FA associated vinculin staining, particularly at the periphery of the cells. Projected cell area and the vinculin-containing FA area were also quantified in the middle and right column, respectively. Bars, 50 μm .

10% cyclic stretching. From prior experiments, the ratio of vinculin to total cell area in the unstretched state was 0.105 ± 0.002 (mean \pm SEM). Following cyclic stretching at 10% for 2 min, this area ratio increased to 0.156 ± 0.003 . After 30 min of stretching, however, this ratio returned toward the unstretched level (0.121 ± 0.004), albeit remaining slightly higher.

Since actin filaments make bundles, via a variety of accessory proteins, to bear intracellular stresses (Byers and Fujiwara 1982; Zimmerman et al., 2004), we used force-strain data from single F-actin bundles (Deguchi et al., 2006) isolated from vascular smooth muscle cells to determine the material parameters, c and c_1 (Eqs. 4.7 and 4.8) for F-actin. The first Piola-Kirchhoff stress-stretch relation from their data was described well by $\partial w / \partial \alpha = 656\alpha^2 + 138\alpha - 794$ (10^3 Pa) assuming the radius of the F-actin bundles is 100 nm. The associated best-fit parameters were $c=465.3$ kPa and $c_1=3.160$ for the exponential model and $c=1464.0$ kPa and $c_1=0.7975$ for the Misof model.

Total mass fraction of F-actin in the unstretched state was obtained by fitting force-indentation curves from AFM measurements using Eq. 4.9 along with Eqs. 4.7 and 4.8 and the corresponding material parameters noted above. Thirteen force-indentation curves for unstretched cells whose stiffness values were close to the mean for the unstretched cells (1.30 kPa, which was reported in Na et al. (2006)) were chosen for fitting (Fig. 4.3). In this case, $\phi_n = 0$ and total mass fraction, ϕ_o ($\equiv \phi|_{\text{con}}$), was found to be ~ 0.01 for both models. This value is observed to be $\sim 10\%$ of the measured FA related area ratio (Table 4.1). Assuming the vinculin containing area ratio in Table 4.1 and the

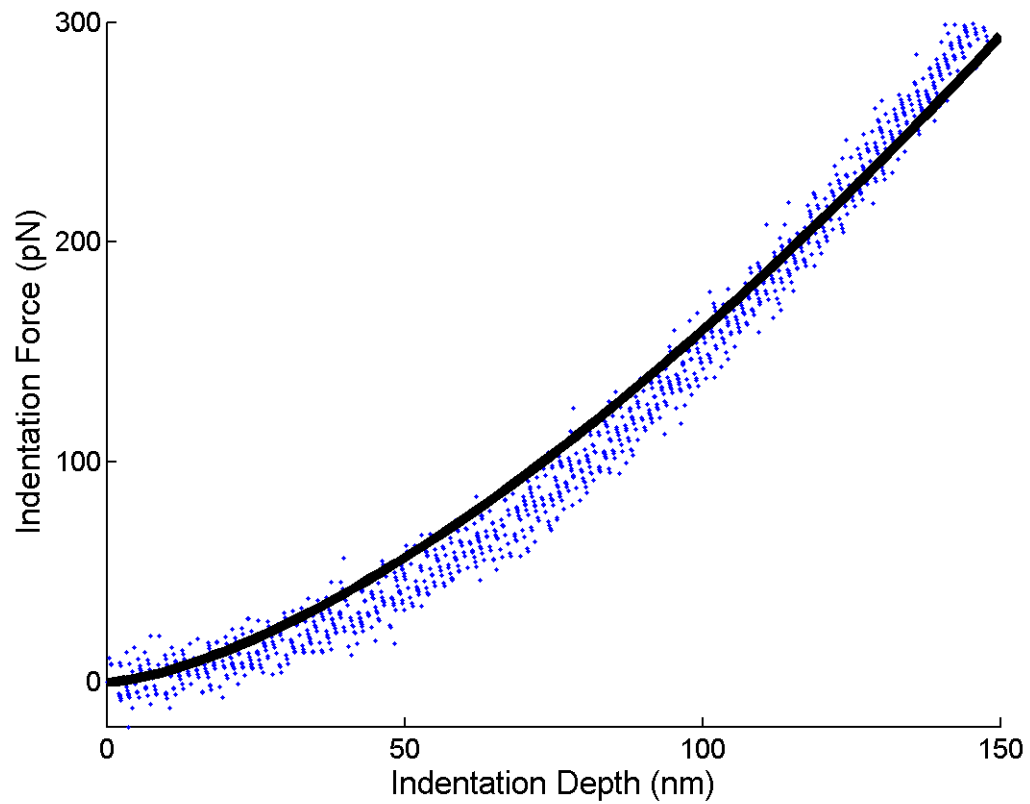


Fig. 4.3. Data from thirteen force-indentation tests obtained from AFM indentations of unstretched cells were fitted with a CSK remodeling model (solid line) to estimate mass fraction of F-actin in unstretched state. Experimental data were chosen from 3 cells over 2 independent experiments.

Table 4.1

FA associated vinculin area ratios and total mass fractions of F-actin in response to 10% cyclic stretching

Stretching Time (min)	FA related Area Ratio ^a	Total F-actin Mass Fraction, ϕ	
		Exponential Model	Misof Model
0	0.105±0.002	0.00979 ^b	0.01102 ^b
2	0.156±0.003	0.01455	0.01637
30	0.121±0.004	0.01128	0.01270

a: FA associated vinculin area ratios were obtained from prior results. N=6~7 cells each for two independent experiments per condition. Results are mean±SEM.

b: Total mass fractions in the unstretched state were obtained from fitting 1 force-indentation curve per cell with a CSK remodeling model. N=5 cells.

mass fraction of F-actin are directly proportional, total mass fractions of F-actin of cells subjected to cyclic stretch were then computed for both models (Table 4.1).

Next, to estimate CSK remodeling during cyclic stretching, data from five force-indentation tests on 5 different cells (one curve for each cell) whose stiffness values were close to the mean values of cell stiffness for each mechanical stretching condition were fit in a similar way to find both ϕ_o and ϕ_n . Mean values of cell stiffness after 2 and 30 min cyclic stretching were 2.42 and 1.46 kPa, respectively (Na et al., 2006). Note, too, that the total mass fraction of F-actin at each mechanical stretching condition is the sum of mass fractions of “original” and “new” F-actin. Hence, following constraints were enforced for the 2 min cyclic stretching condition: $\phi_o|_{2\min} + \phi_n|_{2\min} = \phi|_{2\min}$, $\phi_o|_{2\min} \leq \phi|_{\text{con}}$, $\alpha_n|_{2\min} \geq 1.0$, as well as $1.0 < \alpha_o|_{2\min} \leq 1.1$, where α is the stretch of an F-actin bundle. Constraints for 30 min stretching conditions are similar to those for 2 min. Computed changes in mass fractions and stretch ratios of F-actin following mechanical stretching condition are shown in Fig. 4.3. Whereas the initial mass fractions of F-actin were

$\phi|_{con} \sim 0.01$ in the unstretched state for both models, after 2 min of 10% stretch μ the mass fraction of original F-actin decreased by 60% and 47% for the exponential and Misof model, respectively. Conversely, computed values of the new F-actin were $\phi_n \sim 0.01$ for both models, suggesting that F-actin did remodel in response to cyclic stretching. After 30 min of cyclic stretching, most of the original F-actin was disrupted, as revealed by a computed mass fraction of $\phi_o \sim 0.0016$ for both models, and the mass fraction of the newly polymerized F-actin was $\phi_n \sim 0.01$ for both models (Fig. 4.4A). Stretch ratios computed for the new F-actin following 2 min of cyclic stretching were $\alpha_n \sim 1.03$ and 1.02 (in contrast to $\alpha_o = 1.1$) for the exponential and Misof model, respectively, which decreased to $\alpha_n \sim 1.01$ for both models following 30 min of cyclic stretching (Fig. 4.4B).

In conclusion, the CSK remodeling model based on both the exponential and the Misof relation for F-actin elasticity plus the immunofluorescence and AFM data suggest that cells “produced” new F-actin ($\sim 1\%$ of the total cell mass) soon after the onset of cyclic stretching: at 2 min $\phi_n \sim 0.01$, which were maintained for longer periods of cyclic stretching (Fig. 4.4A), and F-actin had associated different natural configurations whereby the stretch was $\alpha_n \sim 1.03$ after 2 min of stretching but ~ 1.01 after 30 min (Fig. 4.4B).

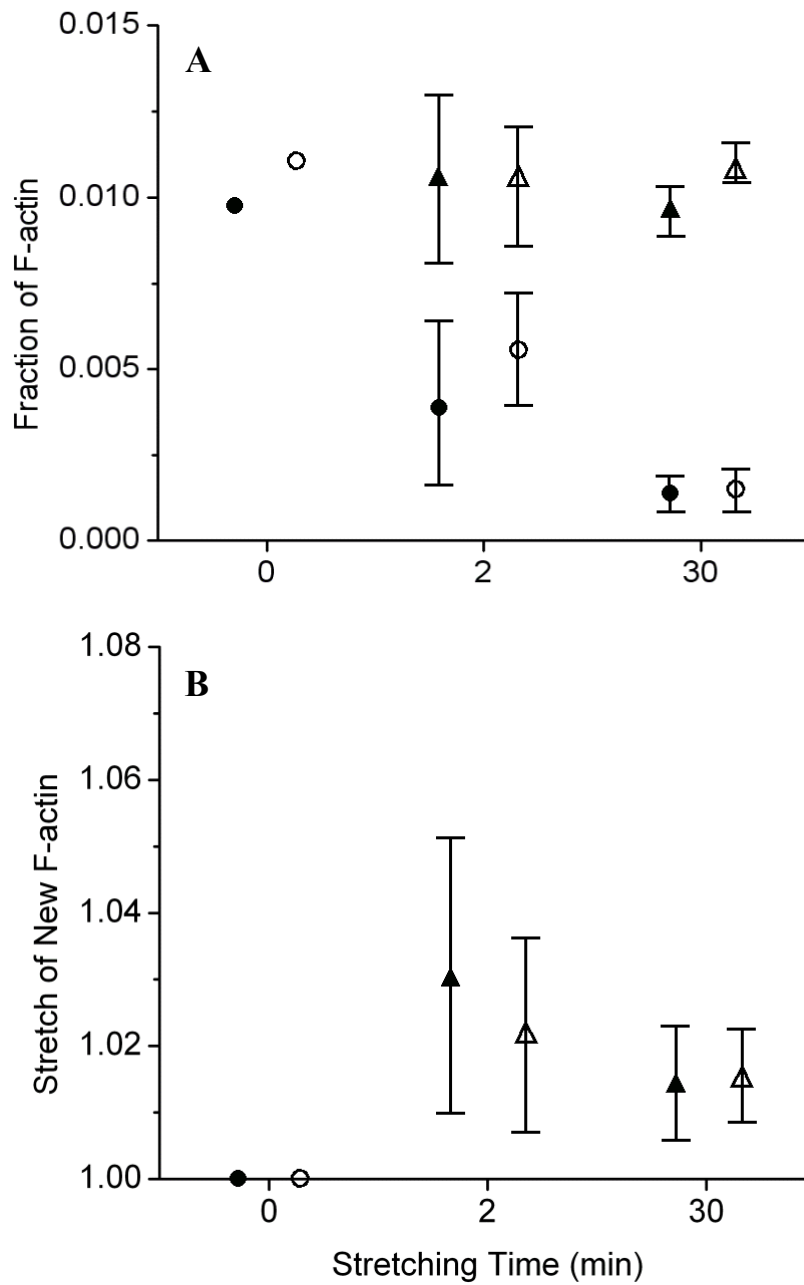


Fig. 4.4. CSK remodeling in response to cyclic stretching. Results show high-low-mean values. ●: original F-actin in the exponential model; ○: original F-actin in the Misof model; ▲: new F-actin in the exponential model; △: new F-actin in the Misof model.

Discussion

The importance of understanding well both cell mechanics and mechanobiology is undisputed, yet significant challenges remain. For a vascular smooth muscle cell (VSMC), for example, we ultimately need to know how the macroscopic loads induced by blood pressure and blood flow within a vessel are distributed throughout the complex cell-matrix structure that defines the vascular wall, how these loads are transferred to particular sites (e.g., at integrins) on the surface of each cell, how these localized loads are distributed within the cytoskeleton (e.g., along actin filaments), and ultimately how these distributed loads affect cell signaling and altered gene expression. Because of the extreme structural complexity over many different length scales – from millimeters at the level of an artery, to microns at the level of collagen fibers and cells, to nanometers at the level of cell surface receptors and CSK constituents – mathematical modeling must range from continuum to microstructural to molecular biomechanics (e.g., see, Stamenović and Ingber, 2002; Humphrey, 2003; Bao and Suresh, 2003; Lim et al., 2006).

Continuum descriptions are well accepted at the vessel level, but can apply at the cellular level as well. For example, characteristic dimensions of a VSMC, on the order of 25 to 100 μm , are much greater than those of the CSK constituents, which are on the order of nm, that endow the cell with its structural integrity and its ability to transduce mechanical signals. Indeed, when one considers the large number of receptors and integrins on a cell surface (on the order of 10^3 to 10^5 ; Lauffenburger and Linderman, 1993), there is further motivation to consider appropriately averaged field quantities.

Finally, formulating continuum level models for both the vessel and the associated cells in parallel with formulations of molecular dynamics models for intracellular constituents will facilitate the development of much needed multi-scale models.

The focus of this chapter is a continuum biomechanical analysis of AFM data on the overall stiffness of cyclically stretched VSMCs in the absence of complexities due to cell-cell and cell-matrix interactions. Whereas most prior AFM data have been collected using nm scale cantilever tips, we suggest that this is inconsistent with the continuum approximations typically used to interpret the associated stiffness data (e.g., the Hertz model). For this reason, we confined our analysis to data collected using larger (5 μm diameter) tips despite having data from both fine and coarse tips (Na et al., 2006). Our results cannot be compared directly to most prior results, therefore, which tend to yield larger estimates of stiffness due to the small tips (e.g., see Fig. 3.5). Moreover, in contrast to most prior continuum models of cells that assume an unchanging materially uniform body, we employed a new constrained mixture model that mass averages contributions of primary CSK constituents, which are allowed to remodel over time. Again, therefore, present results cannot be compared directly to prior results.

Many families of CSK proteins contribute to overall cell stiffness, but F-actin tends to dominate in many situations (Wu et al., 1998a; Smith et al., 2003; Na et al., 2004; Huang et al., 2005;) and thus was the focus herein. There is increasing information available on the elasticity of F-actin, including isolated filaments and networks having different degrees of cross-links (e.g., Liu and Pollack, 2002; Gardel et al., 2004). Best-fit values of material parameters embodied in two different forms of the stored energy

function $w^a(\alpha_i^a)$, $i = \text{“o”}$ or “n” , were determined directly from data in Deguchi et al. (2006) and provided suitable descriptions of the characteristically nonlinear force-length response of bundles of F-actin. Other parameters that contribute to cell stiffness include the mass density, orientation, and cross-linking of the F-actin (Gardel et al., 2004). The present mixture model can capture mass density directly via the evolving mass fraction ϕ_i^a and orientation directly via the potentially evolving distribution function $R_i^a(\varphi, \theta)$; at present, the degree of cross-linking is correlated with the material parameter c , consistent with the results of Gardel et al. (2004). A full evaluation of this general modeling framework, including refinements therein, will clearly require significantly more data on CSK properties and remodeling than is currently available, but this is one use of a theory – to identify and guide needed experiments. Herein, therefore, we simply illustrate potential utility using available data. Actin density was assumed to correlate with FA density, which is to say vinculin or paxillin (Saez et al., 2004), for which data were available. We restricted attention to equibiaxial stretching, which preserves fiber orientations (in plane) and thereby negated the need for detailed analyses of changes in fiber orientations. The original distribution of the actin within the cell was simply assumed to be isotropic relative to some reference configuration (e.g., before the cell adhered and spread). Cross-link density was not monitored, thus we assumed that the material parameters remained constant despite changes in density. Despite these assumptions, Figs. 4.3 and 4.5 reveal that the model was able to fit the overall stiffness data from the AFM reasonably well and thereby supports the general utility of a constrained mixture model for the cell.

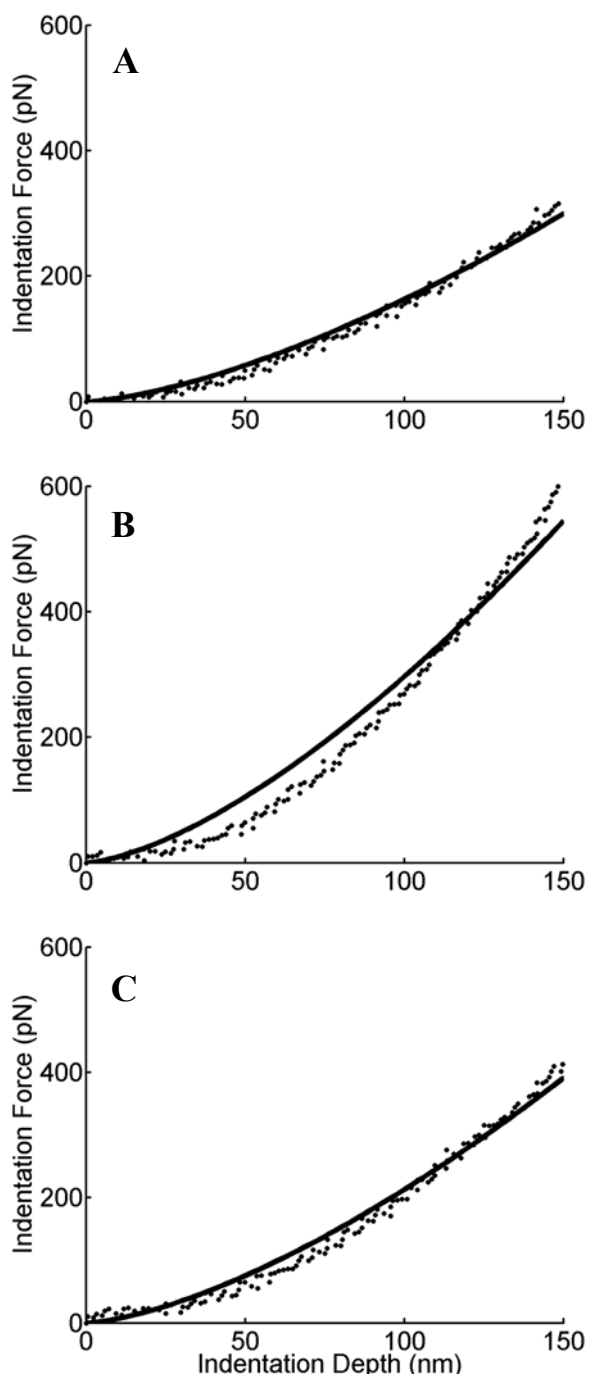


Fig. 4.5. Representative force-indentation curves fitted with AFM indentation measurements obtained from independent experiments: (A) unstretch; (B) 2 min of 10% cyclic stretch; (C) 30 min of 10% cyclic stretch.

It is well known that CSK constituents turnover rapidly in response to perturbations in loading (e.g., Mooney et al., 1995; Galbraith et al., 1998). Although the turnover of F-actin clearly involves depolymerization / repolymerization, the particular changes associated with this turnover remain unknown. Mizutani et al. (2004) recently suggested that just as fibroblasts appear to try to maintain a “tensional homeostasis” in collagen gels in which they are cultured (Brown et al., 1998), so too fibroblasts appear to try to maintain a tensional homeostasis within their CSK. That is, in response to increased (decreased) mechanical loading, cells appear to modify both the extracellular matrix and their cytoskeleton so as to decrease (increase) the stress and thereby restore “normalcy”. Indeed, this concept of a homeostatic tendency is consistent with vessel level responses to increased or decreased stresses (Taber, 1995; Rachev, 2000; Gleason and Humphrey, 2005). The key question, however, is: How does the cell control mechanical homeostasis in different situations? Mizutani et al. found that in response to increased (decreased) uniaxial stretch, fibroblasts exhibited an immediate increase (decrease) in stiffness followed by a gradual (over tens of minutes) return toward the baseline stiffness. As noted above, cell stiffness can be altered by altering actin density, orientation, or cross-linking. In addition, however, we suggest that the ability to depolymerize / repolymerize actin allows the cell to control stiffness by changing the length of the filaments, which is to say by changing their degree of stretch (e.g., since stiffness is stretch dependent). In the context of tissue-level growth and remodeling, this is equivalent to saying that the natural configuration can change for each constituent, which has proved to yield predictions that are consistent with many empirical

observations (Gleason and Humphrey, 2005). Indeed, Fig. 4.4 herein suggests that the acute increase in stiffness in response to an increased cyclic stretch was probably due to an increased stretch of the original filaments whereas the subsequent decrease back towards normalcy was consistent with a replacement of the highly stretched original filaments with less stretched new (i.e., reassembled) filaments. That the stiffness did not return completely to baseline, as in the report by Mizutani et al. (2004), may suggest that the “homeostatic target” is actually an acceptable range (note: Brown et al. (1998) similarly suggest that cells respond only if the perturbation is outside a range of $\pm 25\%$ of normalcy). Albeit measured in endothelial cells, Costa et al. (2002) reported a clever experiment wherein cells were cultured on pre-stretched membranes that could subsequently be relaxed. They found that the actin stress fibers did not buckle, as would be expected of a thin compressed filament, until the membrane shortened significantly. They suggested that a distribution of “pre-extensions” (up to 26%) or pre-stresses exist in the F-actin bundles, which is consistent with the tensional homeostasis concept (Humphrey, 2002a). Clearly, there is a need to quantify this homeostatic stretch in each cell type and filament. Because of the highly nonlinear behavior of F-actin (Janmey et al., 1991; Liu and Pollack, 2002), it appears that small changes in stretch can significantly affect stiffness, restoring it towards its homeostatic range. There is, therefore, a pressing need for experiments to focus on not just the rates of assembly and disassembly, but also the pre-extension in the reassembled filaments in relation to normal values.

In conclusion, we emphasize that, regardless of the type of mathematical model, a disadvantage of most current experimental techniques used to study cell mechanics, including AFM indentation force-depth tests, is that the resulting data are essentially 1-D and fitting such data is not a stringent test of a model. There is, therefore, a need to evaluate this model (as well as other models) using data from multiple experimental set-ups but the same cell conditions. Moreover, just as in tissue level mechanics, we must move towards multi-axial tests of cell mechanics, which provide significantly more information. Finally, because CSK filaments remodel in response to mechanical perturbations, they may well respond locally to changes in loading that are induced by our measurement tools, hence raising the question whether the data actually reflect “native” properties or rapidly “adapted” properties to the local non-physiologic loading. Thus, there is also a need for real-time imaging of CSK changes during mechanical experiments wherein native cell-matrix and cell-cell connections are maintained and the loading on the cell is both multidimensional and more natural.

CHAPTER V

SUMMARY AND CONCLUSIONS

The cytoskeleton is a diverse, multi-protein framework that plays a fundamental role in many cellular activities including mitosis, cell division, intracellular transport, cell motility, muscle contraction, and the regulation of cell polarity and organization (Bray, 2000; Alberts et al., 2002). Furthermore, cytoskeletal filaments have been implicated in the pathogenesis of a wide variety of diseases including cancer, blood disease, cardiovascular disease, inflammatory disease, neurodegenerative disease, and problems with skin, nail, cornea, hair, liver and colon (Ben-ze'ev, 1985; Williamson et al., 1985; Worthen et al., 1989; Bosch et al., 1994; Fuchs and Cleveland, 1998; Towbin 1998; Kirfel et al., 2003). Increasing evidence suggests that the distribution and organization of the cytoskeleton in living cells are affected by mechanical stresses (Smith et al., 1997; Galbraith et al., 1998; Takemasa et al., 1998; Wang et al., 2000, 2001; Hayakawa et al., 2001; Costa et al., 2002; Yoshigi et al., 2003) and the cytoskeleton determines cell stiffness (Wu et al., 1998a; Smith et al., 2003; Huang et al., 2005).

To investigate the effect of mechanical stretching on cytoskeletal remodeling and cell stiffness, we used vascular smooth muscle cells isolated from first order feed arterioles of rat cremaster muscles. Our approach had three components: development of a constrained-mixture based constitutive model for cells to correlate mechanical adaptation with cytoskeletal remodeling; measurement of the time-dependent changes in

focal adhesion localization and cell stiffness in response to cyclic stretching; and estimation of cytoskeletal remodeling by synthesizing data on stretch-induced dynamic changes in cell stiffness and focal adhesion area.

The first objective of this study was to develop a constrained-mixture based constitutive model for cells that can predict cytoskeletal remodeling in response to mechanical stimuli. We developed a fully nonlinear, constrained mixture model for adherent cells that allows one to account separately for the contributions of the primary structural constituents of the cytoskeleton and extended a prior solution from the finite elasticity literature (Green et al., 1952; Beatty and Usmani, 1975) for use in a sub-class of atomic force microscopy studies of cell mechanics. The model showed that the degree of substrate stretch and the geometry of the AFM tip dramatically affect cell stiffness (Costa and Yin, 1999; Na et al., 2004). Consistent with Wakatsuki et al. (2000) and Wu et al. (1998a), the model showed that disruption of the actin filaments can reduce the stiffness substantially, whereas there can be little contribution to the overall cell stiffness by the microtubules or intermediate filaments. Albeit based on a number of simplifying assumptions-e.g., small, quasi-static indentations on equibiaxially stretched cells-the approach proposed here can account for the separate orientations, properties, and deformations of multiple constituents within the cytoskeleton, and, thus, changes in the mechanical response of cells that are induced by biological or mechanical stimuli, such as applying cytoskeleton disrupting drugs or substrate stretching.

The second main objective of this study was to investigate time-dependent changes in smooth muscle cell stiffness and focal adhesion localization in response to

cyclic stretching. We developed a simple cell extension device that can be combined with AFM and confocal microscopy to examine the time course of changes in cell stiffness and cytoskeletal remodeling, respectively. The device applies a cyclic, uniform equibiaxial stretch to a silicone elastic membrane (0.127 mm in thickness) by dynamic infusion and withdrawal of air using a programmable syringe pump. The overall dimensions of the device are 5.3 cm in diameter and 1.6 cm high, which allows it to be secured on the stage of an AFM using a magnetic ring that holds the device in place. Calibration results of the device showed that it could produce a near homogeneous and equibiaxial stretch, particularly in the central 40% of the membrane.

To examine the effect of AFM tip geometry, three types of non-functionalized tips (a pyramidal shape with opening angle of 70° , a $2\ \mu\text{m}$ diameter spherical bead, and a $5\ \mu\text{m}$ diameter bead) were used. The mean stiffness value obtained from 2 or $5\ \mu\text{m}$ diameter bead-attached tips was very stable compared to that obtained from pyramidal shaped tip and $\sim 2\ \text{kPa}$, which was very similar to the range ($0.1\sim 10\ \text{kPa}$) obtained from most other techniques for mechanically probing cells.

To investigate time-dependent changes in smooth muscle cell stiffness, a total of 15 to 25 cells were selected during 2 to 5 independent experiments for each mechanically stimulated condition, which is defined by each combination of 0.25 Hz cyclic stretch of $\mu=1.05$ or 1.1 , and durations of cyclic stretching of 0, 1, 2, 5, 15, 30, 60 min in each experiment. A 5% cyclic stretching yielded no significant change in stiffness despite a slight increase after 1 and 2 min of stretching. In contrast, a 10% cyclic

stretching induced a significant increase in stiffness that was highest after 2 min and returned thereafter towards baseline after 5 min of stretching.

Additional experiments using immunofluorescence staining and confocal microscopy were performed to test whether cytoskeletal remodeling is correlated with the changes in cell stiffness. Consistent with biochemical data from Cunningham et al. (2002), cyclic stretching induced rapid changes in focal adhesion localization. Cells subjected to 10% cyclic stretching for 2 min exhibited a significant increase in focal adhesion area compared to unstretched cells. Therefore, there was a close relationship between stretch induced increases in cell stiffness and area ratio corresponding to focal adhesion associated vinculin and paxillin. In summary, this study demonstrates that cyclic stretching significantly and rapidly alters both cell stiffness and focal adhesion associated vinculin and paxillin. That cell stiffness correlated well with focal adhesion remodeling suggested that focal adhesion remodeling plays a critical role in cell stiffness by recruiting and anchoring F-actin.

The third objective of this study was to estimate cytoskeletal remodeling by synthesizing data on stretch-induced dynamic changes in cell stiffness and focal adhesion area using the aforementioned constrained mixture approach. In contrast to most prior cell mechanics models that assume an unchanging materially uniform body, we employed a new constrained mixture model that mass averages contributions of primary cytoskeletal constituents, which are allowed to remodel over time. Force-indentation data obtained from AFM tests on cells whose stiffness values were close to the mean values of cell stiffness for each mechanical stretching condition were fit with a

mixture model. Here, actin density was assumed to correlate with focal adhesion density. We restricted attention to equibiaxial stretching, which preserves fiber orientations (in plane) and thereby negated the need for detailed analyses of changes in fiber orientations. Cross-link density was not monitored, thus we assumed that the material parameters remained constant despite changes in density. Despite these assumptions, the model was able to fit the overall stiffness data from the AFM reasonably well and thereby supports the general utility of a constrained mixture model for the cell. Results suggest that the acute increase in stiffness in response to an increased cyclic stretch was probably due to an increased stretch of the original filaments whereas the subsequent decrease back towards normalcy was consistent with a replacement of the highly stretched original filaments with less stretched (i.e., reassembled) new filaments.

In conclusion, regardless of the type of mathematical model, a disadvantage of most current experimental techniques used to study cell mechanics, including AFM indentation force-depth tests, is that the resulting data are essentially 1-D and fitting such data is not a stringent test of a model. There is, therefore, a need to evaluate this model (as well as other models) using data from multiple experimental set-ups but the same cell conditions. Finally, because CSK filaments remodel in response to mechanical perturbations, they may well respond locally to changes in loading that are induced by our measurement tools, hence raising the question whether the data actually reflect “native” properties or rapidly “adapted” properties to the local non-physiologic loading. Thus, there is also a need for real-time imaging of CSK changes during mechanical

experiments wherein native cell-matrix and cell-cell connections are maintained and the loading on the cell is both multidimensional and more natural.

REFERENCES

- Alberts, B., Johnson, A., Lewis, J., Raff, M., Roberts, K., Walter, P., 2002. *Molecular Biology of the Cell*. Garland Science, New York.
- Albinsson, S., Nordstrom I., Hellstrand P., 2004. Stretch of the vascular wall induces smooth muscle differentiation by promoting actin polymerization. *Journal of Biological Chemistry* 279, 34849-34855.
- Ashkin, A., Dziedzic, J.M., 1987. Optical trapping and manipulation of viruses and bacteria. *Science* 235, 1517-1520.
- Baek, S., Rajagopal, K.R., Humphrey, J.D., 2006. A theoretical modeling of enlarging intracranial fusiform aneurysms. *ASME Journal of Biomechanical Engineering* 128, 142-149.
- Bao, G., Suresh, S., 2003. Cell and molecular mechanics of biological materials. *Nature Materials* 2, 715-725.
- Beatty, M.F., Usmani, S.A., 1975. On the indentation of a highly elastic half-space. *Quarterly Journal of Mechanics and Applied Mathematics* 28, 47-62.
- Ben-ze'ev, A., 1985. The cytoskeleton in cancer cells. *Biochimica et Biophysica Acta* 780, 197-212.
- Boey, S.K., Boal, D.H., Discher, D.E., 1998. Simulations of the erythrocyte cytoskeleton at large deformation. 1. Microscopic models. *Biophysical Journal* 75, 1573-1583.
- Bosch, F.H., Werre, J.M., Schipper, L., Roerdinkholder-Stoelwinder, B., Huls, T., Willekens, F.L., Wichers, G., Halie, M.R., 1994. Determinants of red blood cell deformability in relation to cell age. *European Journal of Haematology* 52, 35-41.
- Briscoe, B.J., Sebastian, K.S., Adams, M.J., 1994. The effect of indenter geometry on the elastic response to indentation. *Journal of Physics D: Applied Physics* 27, 1156-1162.
- Brodland, G.W., Gordon, R., 1990. Intermediate filaments may prevent buckling of compressively loaded microtubules. *ASME Journal of Biomechanical Engineering* 112, 319-321.

- Butler, J.P., Tolic-Norrelykke, I.M., Fabry, B., Fredberg, J.J., 2002. Traction fields, moments, and strain energy that cells exert on their surroundings. *American Journal of Physiology Cell Physiology* 282, C595-C605.
- Byers, H.R., Fujiwara, K., 1982. Stress fibers in cells in situ: immunofluorescence visualization with antiactin, antimyosin, and anti-alpha-actinin. *Journal of Cell Biology* 93, 804-811.
- Charras, G.T., Horton, M.A., 2002. Single cell mechanotransduction and its modulation analyzed by atomic force microscope indentation. *Biophysical Journal* 82, 2970-2981.
- Cheng, Y., Hartemink, C.A., Hartwig, J.H., Dewey, C.F., 2000. Three-dimensional reconstruction of the actin cytoskeleton from stereo images. *Journal of Biomechanics* 33, 105-113.
- Collins, J.F., Pawloski-Dahm, C., Davis, M.G., Ball, N., Dorn II, G.W., Walsh, R.A., 1996. The role of the cytoskeleton in left ventricular pressure overload hypertrophy and failure. *Journal of Molecular and Cellular Cardiology* 28, 1435-1443.
- Costa, K.D., Yin, F.C.P., 1999. Analysis of indentation: implications for measuring mechanical properties with atomic force microscopy. *ASME Journal of Biomechanical Engineering* 121, 462-471.
- Costa K.D., Hucker W.J., Yin, F.C.P., 2002. Buckling of actin stress fibers: a new wrinkle in the cytoskeletal tapestry. *Cell Motility and the Cytoskeleton* 52, 266-274.
- Cunningham J.J., Linderman, J.J., Mooney, D.J., 2002. Externally applied cyclic strain regulates localization of focal contact components in cultured smooth muscle cells. *Annals of Biomedical Engineering* 30, 927-935.
- Deguchi, S., Ohashi, T., Sato, M., 2006. Tensile properties of single stress fibers isolated from cultured vascular smooth muscle cells. *Journal of Biomechanics*, in press.
- Deng, L., Fairbank, N.J., Fabry, B., Smith, P.G., Maksym, G.N., 2004. Localized mechanical stress induces time-dependent actin cytoskeletal remodeling and stiffening in cultured airway smooth muscle cells. *American Journal of Physiology Cell Physiology* 287, C440-C448.

- Evans, E., Yeung, A., 1989. Apparent viscosity and cortical tension of blood granulocytes determined by micropipet aspiration. *Biophysical Journal* 56, 151-160.
- Fabry, B., Maksym, G.N., Butler, J.P., Glogauer, M., Navajas, D., Fredberg, J.J., 2001. Scaling the microrheology of living cells. *Physical Review Letters* 87(14), 148102.
- Felder, S., Elson, E.L., 1990. Mechanics of fibroblast locomotion: quantitative analysis of forces and motions at the leading lamellas of fibroblasts. *Journal of Cell Biology* 111, 2513-2526.
- Fisher, N.I., Lewis, T., Embleton, B.J.J., 1987. *Statistical Analysis of Spherical Data*. Cambridge University Press, Cambridge.
- Forgacs, G., 1995. On the possible role of cytoskeletal filamentous networks in intracellular signaling: an approach based on percolation. *Journal of Cell Science* 108, 2131-2143.
- Fuchs, E., Cleveland, D.W., 1998. A structural scaffolding of intermediate filaments in health and disease. *Science* 279, 514-519.
- Fung, Y.C., 2002. Celebrating the inauguration of the journal: *Biomechanics and Modeling in Mechanobiology*. *Biomechanics and Modeling in Mechanobiology* 1, 3-4.
- Galbraith, C.G., Skalak, R., Chien, S., 1998. Shear stress induces spatial reorganization of the endothelial cell cytoskeleton. *Cell Motility and the Cytoskeleton* 40, 317-330.
- Gardel, M.L., Shin, J.H., MacKintosh, F.C., Mahadevan, L., Matsudaira, P., Weitz, D.A., 2004. Elastic behavior of cross-linked and bundled actin networks. *Science* 304, 1301-1305.
- Goldmann, W.H., Galneder, R., Ludwig, M., Xu, W., Adamson, E.D., Wang, N., Ezzel, R.M., 1998. Differences in elasticity of vinculin-deficient F9 cells measured by magnetometry and atomic force microscopy. *Experimental Cell Research* 239, 235-242.
- Goldschmidt, M.E., McLeod, K.J., Taylor, W.R., 2001. Integrin-mediated mechano-transduction in vascular smooth muscle cells: frequency and force response characteristics. *Circulation Research* 88, 674-680.

- Green, A.E., Rivlin, R.S., Shield, R.T., 1952. General theory of small elastic deformations superimposed on finite elastic deformations. *Proceedings of Royal Society of London* 211A, 128-154.
- Hayakawa, K., Sato, N., Obinata, T., 2001. Dynamic reorientation of cultured cells and stress fibers under mechanical stress from periodic stretching. *Experimental Cell Research* 268, 104-114.
- Heidemann, S.R., Kaech, S., Buxbaum, R.E., Matus, A., 1999. Direct observations of the mechanical behaviors of cytoskeleton in living fibroblasts. *Journal of Cell Biology* 145, 109-122.
- Herant, M., Marganski, W.A., Dembo, M., 2003. The mechanics of neutrophils: synthetic modeling of three experiments. *Biophysical Journal* 84, 3389-3413.
- Hochmuth, R. M., 2000. Micropipette aspiration of living cells. *Journal of Biomechanics* 33, 15-22.
- Huang, H., Kamm, R.D., Lee, R.T., 2004. Cell mechanics and mechano-transduction: pathways, probes, and physiology. *American Journal of Physiology Cell Physiology* 287, C1-C11.
- Huang, H., Sylvan, J., Jonas, M., Barresi, R., So, P.T.C., Campbell, K.P., Lee, R.T., 2005. Cell stiffness and receptors: evidence for cytoskeletal subnetworks. *American Journal of Physiology-Cell Physiology* 288, C72-C80.
- Humphrey, J.D., Vawter, D.L., Vito, R.P., 1987. Quantification of strains in biaxially tested soft tissues. *Journal of Biomechanics* 20, 59-65.
- Humphrey, J.D., Yin, F.C.P., 1987. A new constitutive formulation for characterizing the mechanical behavior of soft tissues. *Biophysical Journal* 52, 563-570.
- Humphrey, J.D., Halperin, H.R., Yin, F.C.P., 1991. Small indentation superimposed on a finite equibiaxial stretch: implications for cardiac mechanics. *ASME Journal of Applied Mechanics* 58, 1108-1111.
- Humphrey, J.D., 2002a. On mechanical modeling of dynamic changes in the structure and properties of adherent cells. *Mathematics and Mechanics of Solids* 7, 521-539.

- Humphrey, J.D., 2002b. *Cardiovascular Solid Mechanics: Cells, Tissues, and Organs*, Springer-Verlag, New York.
- Ingber, D.E., 1993. Cellular tensegrity: defining new rules of biological design that govern the cytoskeleton. *Journal of Cell Science* 104, 613-627.
- Janmey, P.A., Euteneuer, U., Traub, P., Schliwa, M., 1991. Viscoelastic properties of vimentin compared with other filamentous biopolymer networks. *Journal of Cell Biology* 113, 155-160.
- Kim, B.S., Nikolovski, J., Bonadio, J., Mooney, D.J., 1999. Cyclic mechanical strain regulates the development of engineered smooth muscle tissue. *Nature Biotechnology* 17, 979-983.
- Kirfel, J., T. M. Magin, and J. Reichelt. 2003. Keratins: a structural scaffold with emerging functions. *Cellular and Molecular Life Sciences* 60, 56–71.
- Kuznetsov, Y.G., Malkin, A.J., McPherson, A., 1997. Atomic force microscopy studies of living cells: visualization of motility, division, aggregation, transformation, and apoptosis. *Journal of Structural Biology* 120, 180-191.
- Lanir, Y., 1983. Constitutive equations for fibrous connective tissues. *Journal of Biomechanics* 12, 423-436.
- Lauffenburger, D.A., Linderman, J.J., 1993. *Receptors: Models for Binding, Trafficking, and Signaling*. Oxford University Press, Oxford.
- Li, C., Xu, Q., 2000. Mechanical stress-initiated signal transductions in vascular smooth muscle cells. *Cellular Signaling* 12, 435-445.
- Lim, C.T., Zhou, E.H., Quek, S.T., 2006. Mechanical models for living cells-a review. *Journal of Biomechanics* 39, 195-216.
- Liu, X., Pollack, G.H., 2002. Mechanics of F-actin characterized with microfabricated cantilevers. *Biophysical Journal* 83, 2705-2715.
- Mathur, A.B., Collinsworth, A.M., Reichert, W.M., Krauss, W.E., Truskey, G.A., 2001. Endothelial, cardiac muscle and skeletal muscle exhibit different viscous and elastic properties as determined by atomic force microscopy. *Journal of Biomechanics* 34, 1545-1553.

- Misof, K., Rapp, G., Fratzl, P., 1997. A new molecular model for collagen elasticity based on synchrotron X-ray scattering evidence. *Biophysical Journal* 72, 1376-1381.
- Mitra, S.K., Hanson, D.A., Schlaepfer, D.D., 2005. Focal adhesion kinase: in command and control of cell motility. *Nature Reviews Molecular Cell Biology* 6, 56-68.
- Miyazaki, H., Hayashi, K., 1999. Atomic force microscopic measurement of the mechanical properties of intact endothelial cells in fresh arteries. *Medical & Biological Engineering & Computing* 37, 530-536.
- Mizutani, T., Haga, H., Kawabata, K., 2004. Cellular stiffness response to external deformation: tensional homeostasis in a single fibroblast. *Cell Motility and the Cytoskeleton* 59, 242-248.
- Munevar, S., Dembo, M., Wang, Y-L., 2001. Traction force microscopy of normal and transformed fibroblasts. *Biophysical Journal* 80, 1744-1757.
- Na, S., Sun, Z., Meininger, G.A., Humphrey, J.D., 2004. On atomic force microscopy and the constitutive behavior of living cells. *Biomechanics and Modeling in Mechanobiology* 3, 75-84.
- Na, S., Trache, A., Sun, Z., Meininger, G.A., Humphrey, J.D., 2006. Time-dependent changes in smooth muscle cell stiffness and focal adhesion area in response to cyclic stretch. Submitted.
- Pender, N., McCulloch, C.A.G., 1991. Quantitation of actin polymerization in two human fibroblast sub-types responding to mechanical stretching. *Journal of Cell Science* 100, 187-193.
- Radmacher, M., Tillmann, R.W., Fritz, M., Gaub, H.E., 1992. From molecules to cells: imaging soft samples with the atomic force microscope. *Science* 257, 1900-1904.
- Rajagopal, K.R., Tao, L., 1995. *Mechanics of Mixtures*, World Scientific, Singapore.
- Reusch, P., Wagdy, H., Reusch, R., Wilson, E., Ives, H.E., 1996. Mechanical strain increases smooth muscle and decreases nonmuscle myosin expression in rat vascular smooth muscle cells. *Circulation Research* 79, 1046-1053.

- Rotsch, C., Radmacher, M., 2000. Drug-induced changes of cytoskeletal structure and mechanics in fibroblasts: an atomic force microscopy study. *Biophysical Journal* 78, 520-535.
- Saez , A.O., Zhang, W., Wu, Y., Turner, C.E., Tang, D.D., Gunst, S.J., 2004. Tension development during contractile stimulation of smooth muscle requires recruitment of paxillin and vinculin to the membrane. *American Journal of Physiology Cell Physiology* 286, C433-C447.
- Satcher, R.L., Dewey, C.F., 1996. Theoretical estimates of mechanical properties of the endothelial cell cytoskeleton. *Biophysical Journal* 71, 109-118.
- Sato, M., Nagayama, K., Kataoka, N., Sasaki, M., Hane, K., 2000. Local mechanical properties measured by atomic force microscopy for cultured bovine endothelial cells exposed to shear stress. *Journal of Biomechanics* 33, 127-135.
- Sawada, Y., Sheetz, M.P., 2002. Force transduction by triton cytoskeleton. *Journal of Cell Biology* 156, 609-615.
- Schmid-Schönbein, G.W., Kosawada, T., Skalak, R., Chien, S., 1995. Membrane model of endothelial cells and leukocytes. A proposal for the origin of a cortical stress. *Journal of Biomechanical Engineering* 117, 171-178.
- Smith, P.G., Garcia, R., Kogerman, L., 1997. Strain reorganizes focal adhesions and cytoskeleton in cultured airway smooth muscle cells. *Experimental Cell Research* 232, 127-136.
- Smith, P.G., Deng, L., Fredberg, J.J., Maksym, G.N., 2003. Mechanical strain increases cell stiffness through cytoskeletal filament organization. *American Journal of Physiology-Lung Cellular and Molecular Physiology* 285, L456-L463.
- Sneddon, I.N., 1965. The relation between load and penetration in the axisymmetric Boussinesq problem for a punch of arbitrary profile. *International Journal of Engineering Science* 3, 47-57.
- Stamenovic, D., Fredberg, J.J., Wang, N., Butler, J.P., Ingber, D.E., 1996. A microstructural approach to cytoskeletal mechanics based on tensegrity. *Journal of Theoretical Biology* 181, 125-136.

- Stamenovic, D., Ingber, D., 2002. Models of cytoskeletal mechanics of adherent cells. *Biomechanics and Modeling in Mechanobiology* 1, 95-108.
- Sumpio, B.E., Banes, A.J., Levin, L.G., Johnson, G.Jr., 1987. Mechanical stress stimulates aortic endothelial cells to proliferate. *Journal of Vascular Surgery* 6, 252-256.
- Sun, Z., Martinez-Lemus, L.A., Trache, A., Trzeciakowski, J.P., Davis, G.E., Pohl, U., Meininger, G.A., 2005. Mechanical properties of the interaction between fibronectin and $\alpha 5\beta 1$ integrin on vascular smooth muscle cells studied using atomic force microscopy. *American Journal of Physiology Heart and Circulatory Physiology* 289, H2526-H2535.
- Takemasa, T., Yamaguchi, T., Yamamoto, Y., Sutimoto, K., Yamashita, K., 1998. Oblique alignment of stress fibers in cells reduces the mechanical stress in cyclically deforming fields. *European Journal of Cell Biology* 77, 91-99.
- Thubrikar, M.J., Baker, J.W., Nolan, S.P., 1988. Inhibition of atherosclerosis associated with reduction of arterial intramural stress in rabbits. *Arteriosclerosis* 8, 410-420.
- Towbin, J.A., 1998. The role of cytoskeletal proteins in cardiomyopathies. *Current Opinion in Cell Biology* 10, 131-139.
- Treloar, L.R.G., 1975. *The Physics of Rubber Elasticity*. Clarendon Press, Oxford, U.K.
- Truesdell, C., Noll, W., 1965. The non-linear field theories of mechanics. In: Flugge, S. (Ed.), *Handbuch der Physik III*, Springer-Verlag, Berlin, pp. 5.
- Vliet, K.J.V., Bao, G., Suresh, S., 2003. The biomechanics toolbox: experimental approaches for living cells and biomolecules. *Acta Materialia* 51, 5881-5905.
- Wakatsuki, T., Kolodney, M.S., Zahalak, G.I., Elson, E.L., 2000. Cell mechanics studied by a reconstituted model tissue. *Biophysical Journal* 79, 2353-2368.
- Wang, J.H.-C., Goldschmidt-Clermont, P., Moldovan, N., Yin, F.C.-P., 2000. Leukotrienes and tyrosine phosphorylation mediate stretching-induced actin cytoskeletal remodeling in endothelial cells. *Cell Motility and the Cytoskeleton* 46, 137-145.

- Wang, J.H.-C., Goldschmidt-Clermont, P., Wille, J., Yin, F.C.-P., 2001. Specificity of endothelial cell reorientation in response to cyclic mechanical stretching. *Journal of Biomechanics* 34, 1563-1572.
- Wang, N., Butler, J.P., Ingber, D.E., 1993. Mechanotransduction across the cell surface and through the cytoskeleton. *Science* 260, 1124-1127.
- Williamson, J.R., Gardner, R.A., Boylan, C.W., Carroll, G.L., Chang, K., Marvel, J.S., Gonen, B., Kilo, C., Tran-Son-Tay, R., Suter, S.P., 1985. Microrheologic investigation of erythrocyte deformability in diabetes mellitus. *Blood* 65, 283-288.
- Worthen, G. S., Schwab 3rd, B., Elson, E.L., Downey, G.P., 1989. Mechanics of stimulated neutrophils: cell stiffening induces retention in capillaries. *Science* 245, 183-186.
- Wu, H.W., Kuhn, T., Moy, V.T., 1998a. Mechanical properties of L929 cells measured by atomic force microscopy: effects of anticytoskeletal drugs and membrane crosslinking. *Scanning* 20, 389-397.
- Wu, X., Mogford, J.E., Platts, S.H., Davis, G.E., Meininger, G.A., Davis, M.J., 1998b. Modulation of calcium current in arteriolar smooth muscle by α v β 3 and α 5 β 1 integrin ligands. *Journal of Cell Biology* 143, 241-252.
- Yoshigi, M., Clark, E.B., Yost, H.J., 2003. Quantification of stretch-induced cytoskeletal remodeling in vascular endothelial cells by image processing. *Cytometry Part A* 55A, 109-118.
- Yoshigi, M., Hoffman, L.M., Jensen, C.C., Yost, H.J., Beckerle, M.C., 2005. Mechanical force mobilizes zyxin from focal adhesions to actin filaments and regulates cytoskeletal reinforcement. *Journal of Cell Biology* 171, 209-215.
- Zhu, C., Bao, G., Wang, N., 2000. Cell mechanics: mechanical response, cell adhesion, and molecular deformation. *Annual Review of Biomedical Engineering* 2, 189-226.
- Zimmerman, B., Volberg, T., Geiger, B., 2004. Early molecular events in the assembly of the focal adhesion-stress fiber complex during fibroblast spreading. *Cell Motility and the Cytoskeleton* 58, 143-159.

APPENDIX

Assume that, in cylindrical coordinates, when the membrane is stretched equibiaxially, it has an isochoric, axisymmetric, and homogeneous deformation of the form, namely, $r = \mu R, \theta = \Theta, z = Z$, where (R, Θ, Z) and (r, θ, z) are particle coordinates of an unstretched reference and stretched configuration, respectively, with μ and λ constants at each stretch. Hence, the physical components of deformation gradient \mathbf{F} are

$$[\mathbf{F}] = \begin{bmatrix} \partial r / \partial R & 0 & 0 \\ 0 & r/R & 0 \\ 0 & 0 & \lambda \end{bmatrix} = \begin{bmatrix} \mu & 0 & 0 \\ 0 & \mu & 0 \\ 0 & 0 & \lambda \end{bmatrix}, \quad (\text{A1})$$

with $\lambda = 1/\mu^2$ from the assumed incompressibility requiring $\det \mathbf{F} = 1$. Since the membrane is very thin, we can reduce \mathbf{F} for 3-D to that for 2-D. Now, therefore, consider 2-D with

$$[\mathbf{F}_{2D}] = \begin{bmatrix} \beta & 0 \\ 0 & \beta \end{bmatrix}. \quad (\text{A2})$$

Cartesian coordinates are obtained by rotating the cylindrical coordinates by an angle $\hat{\theta}$ about the axis perpendicular to the membrane. Thus,

$$\mathbf{e}_x = \cos \hat{\theta} \mathbf{e}_r + \sin \hat{\theta} \mathbf{e}_\theta, \quad \mathbf{e}_y = -\sin \hat{\theta} \mathbf{e}_r + \cos \hat{\theta} \mathbf{e}_\theta. \quad (\text{A3})$$

The left Cauchy-Green tensor in the Cartesian coordinate system, which is defined by

$\bar{\mathbf{B}} = \bar{\mathbf{F}}_{2D} \bar{\mathbf{F}}_{2D}^T$, is defined as follows:

$$\bar{B}_{ij} = A_{ik} A_{jl} B_{kl} \quad \text{or} \quad \bar{\mathbf{B}} = \mathbf{A} \mathbf{B} \mathbf{A}^T, \quad (\text{A4})$$

where $[\mathbf{A}] = \begin{bmatrix} \cos \hat{\theta} & \sin \hat{\theta} \\ -\sin \hat{\theta} & \cos \hat{\theta} \end{bmatrix}$ and \mathbf{B} is the left Cauchy-Green tensor in the cylindrical

coordinate system. Substituting \mathbf{A} into Eq. (A4) gives

$$\begin{bmatrix} \bar{B}_{11} & \bar{B}_{12} \\ \bar{B}_{21} & \bar{B}_{22} \end{bmatrix} = \begin{bmatrix} \cos \hat{\theta} & \sin \hat{\theta} \\ -\sin \hat{\theta} & \cos \hat{\theta} \end{bmatrix} \begin{bmatrix} B_{11} & B_{12} \\ B_{21} & B_{22} \end{bmatrix} \begin{bmatrix} \cos \hat{\theta} & -\sin \hat{\theta} \\ \sin \hat{\theta} & \cos \hat{\theta} \end{bmatrix}. \quad (\text{A5})$$

Thus,

$$\begin{aligned} \bar{B}_{11} &= B_{11} \cos^2 \hat{\theta} + B_{22} \sin^2 \hat{\theta}, \\ \bar{B}_{12} &= -B_{11} \sin \hat{\theta} \cos \hat{\theta} + B_{22} \sin \hat{\theta} \cos \hat{\theta}, \\ \bar{B}_{22} &= B_{11} \sin^2 \hat{\theta} + B_{22} \cos^2 \hat{\theta}, \end{aligned} \quad (\text{A6})$$

with $\bar{B}_{21} = \bar{B}_{12}$.

Since $B_{11} = B_{22} = \beta^2$ in this problem,

$$\bar{B}_{11} = B_{11} = B_{22} = \bar{B}_{22} \quad \text{with} \quad \bar{B}_{12} = \bar{B}_{21} = 0. \quad (\text{A7})$$

Therefore, components of deformation gradient in cylindrical coordinates are same as those in Cartesian coordinates and the deformation is equibiaxial.

VITA

Name: Sungsoo Na

Address: 337 Zachry Engineering Center, 3120 TAMU, Biomedical Engineering department, College Station, TX 77843-3120

Education: B.S., Mechanical Engineering, Pukyong National University, 1993
M.S., Mechanical Engineering, Pusan National University, 2000
Ph.D., Biomedical Engineering, Texas A&M University, 2006

Awards and honors:

Fred J. Benson Graduate Fellowship, Texas A&M University, 2000-2001
BMES 2004 Poster Award, BMES Conference, Philadelphia, PA, 2004

Journal publications:

Humphrey, J.D., Na, S., 2002. Elastodynamics and arterial wall stress. *Annals of Biomedical Engineering* 30, 509-523.

Na, S., Sun, Z., Meininger, G.A., Humphrey, J.D., 2004. On atomic force microscopy and the constitutive behavior of living cells. *Biomechanics and Modeling in Mechanobiology* 3, 75-84.

In-Preparation

Na, S., Trache, A., Sun, Z., Meininger, G.A., Humphrey, J.D., Time-dependent changes in cell stiffness and focal adhesion localization in response to cyclic stretch.

Na, S., Meininger, G.A., Humphrey, J.D., Time-dependent changes in cytoskeletal remodeling in response to cyclic stretch: a theoretical study based on experimental data.

Journal Reviewer:

ASME Journal of Biomechanical Engineering
Biomechanics and Modeling in Mechanobiology